DANISH METEOROLOGICAL INSTITUTE

——— SCIENTIFIC REPORT ———

98-1

HIRLAM 2.5 parallel tests at DMI: Sensitivity to type of schemes for turbulence, moist processes and advection

Niels Woetmann Nielsen
Bjarne Amstrup
Jess U. Jørgensen

DMI

COPENHAGEN 1998

ISSN-Nr. 0905-3263
ISBN-Nr. 87-7478-366-1

HIRLAM 2.5 parallel tests at DMI: Sensitivity to type of schemes for turbulence, moist processes and advection

Niels Woetmann Nielsen, Bjarne Amstrup and Jess U. Jørgensen
Danish Meteorological Institute, Copenhagen, Denmark

1. Introduction

Results from a series of parallel experiments are presented in the present report. They show, in terms of objective verification scores and in terms of case study evaluations, the impact of changes in forecast system components ranging from dynamics to physics. In order to obtain reliable statistics five periods (P1 to P5) giving a total of 65 days, representing three years and all seasons, have been selected for the experiments. Information about the periods P1 to P5, including their length in days, is given in Table 1. The basic model applied in the experiments is DMI-HIRLAM-G, which was the outer component of the operational nested model system at DMI until September 1997. The experiments have been designed such that only one model change has been made at a time. This has been done to eliminate ambiguity in the interpretation of the results. The operational forecasting system at DMI is briefly described in section 2. This section also contains information about the modification to the basic model (DMI-HIRLAM-G) introduced in each of the parallel experiments studied in the present report.

Table 1: Definition of periods.

Period	Year	Start			End			Number
		month	day	hour	month	day	hour	of days
P1	94	09	11	00	09	22	18	12
P2	95	10	25	00	11	08	18	15
P3	97	01	28	00	02	11	00	15
P4	97	04	02	00	04	14	06	13
P5	97	06	22	12	07	02	06	10

The results presented in section 3 show the impact of replacing a local with a nonlocal first order vertical diffusion scheme.

In section 4 results obtained with three different condensation schemes are intercompared. The applied schemes are the Kuo/Cond scheme (part of the basic model), the Sundqvist scheme (Sundqvist et al., 1989; Sundqvist, 1993) and the STRACO scheme (Sass, 1997). The latter scheme is a modified Sundqvist scheme. Contrary to the Sundqvist scheme it contains a soft transition between the convective and stratiform regimes. Experiments have shown that the latter leads to a significant damping of the numerical noise on the smallest resolvable scales of the model.

A semi-Lagrangian advection scheme has been developed in the HIRLAM 3 period as a computationally economic alternative to the Eulerian advection scheme applied in the operational system at DMI.

In section 5 results of the Eulerian experiments presented in section 4 are intercompared with corresponding semi-Lagrangian experiments.

Section 6 contains a discussion of the results and finally a summary of the main conclusions drawn from the parallel experiments is given in section 7.

2. Model-system

The basic model applied in the present parallel experiments is DMI-HIRLAM-G, built on reference version HIRLAM 2.5.7 (Källén, 1996), with the specific DMI updates listed in the Appendix. This model was the outer component of the operational nested model-system at DMI until September 1997. Its integration domain covers Europe, the northern North Atlantic and parts of the Polar Sea, Canada and USA.

In Table 2 the experiment performed with the basic model (DMI-HIRLAM-G) has been labeled CBC. The table also contains a list of labels for the other parallel experiments studied in the present report, together with details about the circumstances under which they have been performed. As indicated by the second column in Table 2 only one model change has been made between each parallel experiment. The latter eliminates ambiguity in the interpretation of the results. For identification reasons the experiments are sometimes referenced in the text as CBC(opr-eu), CBD(kuo-eu), CBE(sun-eu), CBJ(str-eu), CBF(kuo-sl), CBG(sun-sl) and CBK(str-sl).

Table 2: Definition of experiments.

Name of exp.	DMI-HIRLAM-G variant	Type of advection	Horizontal diff. coeff.	Horizontal diff. type	Time step in seconds
CBC	KUO/COND+VDIF	Euler	10^{14}	4. order, expl.	240
CBD	KUO/COND+NLVDIF	Euler	10^{14}	4. order, expl.	240
CBE	SUNDQVIST+NLVDIF	Euler	10^{14}	4. order, expl.	240
CBJ	STRACO+NLVDIF	Euler	10^{14}	4. order, expl.	240
CBF	KUO/COND+VDIF	Semil.	10^{24}	6. order, impl.	720
CBG	SUNDQVIST+NLVDIF	Semil.	10^{24}	6. order, impl.	720
CBK	STRACO+NLVDIF	Semil.	10^{24}	6. order, impl.	720
Additional information valid for all experiments:					
	Data assimilation frequency: 6 hours				
	Boundary values: ECMWF analyses				
	Boundary update frequency: 6 hours				
	Horizontal resolution: $0.42^\circ \times 0.42^\circ$				
	Vertical resolution: 31 levels				
	Size of domain: nlon = 194, nlat = 163.				

3. Local versus nonlocal first order vertical diffusion

In this and sections 4 and 5 the assessment of the quality of the parallel experiments is based on objective verification scores and subjective evaluation of individual forecasts. The statistical tools are verification against observations (obs-verification) and field verification.

The list of observations applied in the obs-verification is an extended EWGLAM-list with inclusion of observations from the northern North Atlantic and Greenland. The presented scores for the obs-verification are bias and root mean square (rms) error, while the scores for the field verification are bias and standard deviation (std. dev.) error of the forecast minus its own verifying analysis field.

In this section results from experiments CBC and CBD are intercompared. According to Table 2 the experiments only differ with respect to the applied vertical diffusion scheme. CBC has been run with a first order local diffusion scheme (Källén, 1996; Louis et al., 1981). In CBD the latter scheme has been replaced by a first order nonlocal scheme (Nielsen and Sass, 1995), which is a modified version of the scheme by Holtslag and Boville, 1993.

3.1. Obs-verification

Average values of the obs-verification scores for periods P1 to P5 are shown in Figures 1 to 4 for selected parameters. It is shown by the figures that the rms errors for CBD are slightly smaller than for CBC. The only exception is the 850 hPa temperature (Figure 3, top). The bias is in general numerically smallest in CBD, in particular for 2 m temperature (Figure 1, middle) and 850 hPa temperature (Figure 3, top). For mean sea level pressure (mslp) the bias is slightly more negative in CBD.

The pattern shown by the mean scores for the five periods is generally also valid for the individual periods, although considerable variations in both bias and rms error occur between the periods (figures not shown). Part of the variation is undoubtly due to the seasonal variation in the intensity of the general circulation. Another part is likely to be due to inter-annual variability in the prevailing seasonal flow pattern.

From the obs-verification results in Figures 1 to 4 it can be concluded that a small improvement in forecast quality is obtained by switching from the first order local vertical diffusion scheme in CBC to a corresponding nonlocal scheme in CBD.

3.2. Field verification

Field verification is another tool for measuring forecast quality. Field verification scores for CBC and CBD are summarized in the two rightmost columns of Table 3. The numbers are sums of individual scores obtained by assigning bias score +1 to the experiment (in each case) with the numerically smallest bias and by assigning std. dev. error score +1 to the experiment with the smallest std. dev. error. The scores in Table 3 are determined from the qualitative measures of bias and std. dev. error for each case listed in columns 2 to 3 and 4 to 5, respectively. Symbols e, s and ℓ mean 'equal', 'smallest' and 'largest', respectively. The sign of the bias is indicated by + and −. A near-zero bias is indicated by 0.

According to the numbers above the bias is best in CBC in 40% of the cases (a case is here defined by parameter and period). The corresponding number for CBD is 29%. For the std. dev. error CBD is best in 42% of the cases, while CBC only is best in 22% of the cases.

The bias and std. dev. errors of the parameters in Table 3 have considerable geographical variation. An example is presented in Figure 5a, showing the average mslp

together with the std. dev. error of mslp for CBC in period P3. For the same period the difference in std. dev. error of mslp between CBC and CBD is shown in Figure 5b. It can be seen that positive differences occur in most of the integration domain. This is consistent with the result in Table 3, column 5.

From the field verification results summarized in Table 3 together with Figures 5a and 5b it can be concluded that relative to CBC the CBD forecasts are marginally worse in terms of bias, but somewhat better in terms of std. dev. error. The similarity with the obs-verification results is clear, in particular for bias of 850 hPa temperature and std. dev. error of mslp and height fields at 850, 500 and 250 hPa.

3.3. Case studies

The last component in the evaluation of the results of the parallel experiments is subjective assessment of forecasts on selected days. For practical reasons the number of cases has been limited to four, with one case in each of the periods P1, P3, P4 and P5, representing autumn, winter, spring and summer, respectively. Furthermore, only forecasts of mslp are considered. The forecast length is 48 hours for the three first cases, but because of one missing 48 hours forecast (CBE) in the archive, the forecast length in the summer case is only 36 hours.

The general criterion for the selection of cases has been that all seasons should be represented, and that each case should have one or more elements of extreme weather. For the selected cases the elements of extreme weather are respectively heavy rainfall, intense marine cyclogenesis, spring snowfall in Denmark and summer cyclogenesis with severe convection.

The autumn and winter forecasts together with the verifying CBC analyses are shown in Figure 6. In the autumn case strong cyclogenesis has taken place over northern Germany and the Netherlands. The position of the center of the cyclone is rather well predicted by both model versions, but the depth and shape of the low in the CBD forecast is in slightly better agreement with the verifying CBC analysis.

The autumn case represents a 'high predictability' group of forecasts, where different model versions tend to produce only slightly different forecasts. For such cases the differences between two forecasts tend to be small and of the same magnitude as 'forecast minus verifying analysis' differences.

In the winter case 'explosive' cyclogenesis has occurred over the sea between Iceland and Norway. It is shown by Figure 6 (right column) that both the depth and position of the low is poorly predicted by both model versions, although the position and depth of the cyclone is slightly better predicted by CBD.

The winter case represents a 'low predictability' group of forecasts. In such cases both differences between forecasts produced by different model versions and differences between forecast and verifying analysis can be very large.

In the spring case (Figure 7, left column) a small scale low has been steered by a mid-tropospheric northwesterly flow to the North Sea. Both the shape, position and depth of the low is clearly best predicted by CBD. It can for example be noted that in CBD the depth is approximately as analysed, while in CBC the low is between 8 and 10 hPa deeper than analysed.

In the summer case relatively intense cyclogenesis has occurred over the North Sea.

Table 3: Local vdiff versus nonlocal vdiff.

	CBC					CBD					CBC					CBD					Σ(bias)		Σ(std. dev.)	
param	bias scores					bias scores					std. dev. scores					std. dev. scores					C	D	C	D
period	P1	P2	P3	P4	P5	P1	P2	P3	P4	P5	P1	P2	P3	P4	P5	P1	P2	P3	P4	P5				
mslp	ℓ+	s0	s0	ℓ+	ℓ+	s+	ℓ−	ℓ−	s+	s+	ℓ	ℓ	ℓ	ℓ	s	s	s	s	s	ℓ	3+	2+	1+	4+
RH-850	s−	s−	s−	e−	e−	ℓ−	ℓ−	ℓ−	e−	e−	e	e	e	e	ℓ	e	e	e	e	s	3+	0	0	1+
RH-500	e+	e+	s+	e+	e0	e+	e+	ℓ+	e+	e0	s	e	s	e	ℓ	ℓ	e	ℓ	e	s	1+	0	2+	1+
H-850	s+	e−	s−	e+	e−	ℓ+	e−	ℓ−	e+	e−	ℓ	ℓ	ℓ	ℓ	s	s	s	s	s	ℓ	2+	1+	1+	4+
H-500	ℓ−	ℓ−	e−	ℓ−	e−	s−	s−	e−	s−	e−	ℓ	ℓ	e	ℓ	e	s	s	e	s	e	0	3+	0	3+
H-250	ℓ−	e−	s−	e−	s−	s−	e−	ℓ−	e−	ℓ−	ℓ	ℓ	ℓ	ℓ	e	s	s	s	s	e	2+	1+	0	4+
T-850	ℓ−	ℓ−	ℓ−	ℓ−	ℓ−	s−	ℓ+	s−	s−	s−	ℓ	s	s	e	ℓ	s	ℓ	ℓ	e	s	0	5+	2+	2+
T-500	s−	e−	s−	s−	e−	ℓ−	e−	ℓ−	ℓ−	e−	e	e	e	e	s	e	e	e	e	ℓ	3+	0	1+	0
T-250	s0	s−	s−	s−	ℓ+	ℓ−	ℓ−	ℓ−	ℓ−	s+	s	s	e	e	s	ℓ	ℓ	e	e	ℓ	4+	1+	3+	0
																			total:		18+	13+	10+	19+

Table 4: Kuo/Cond Euler contra Sundqvist Euler.

	CBD					CBE					CBD					CBE					Σ(bias)		Σ(std. dev.)	
param	bias scores					bias scores					std. dev. scores					std. dev. scores					D	E	D	E
period	P1	P2	P3	P4	P5	P1	P2	P3	P4	P5	P1	P2	P3	P4	P5	P1	P2	P3	P4	P5				
mslp	s+	ℓ−	ℓ−	s+	s+	ℓ+	ℓ+	s0	ℓ+	ℓ+	s	s	s	s	s	ℓ	ℓ	ℓ	ℓ	ℓ	3+	1+	5+	0
RH-850	ℓ−	ℓ−	ℓ−	ℓ−	ℓ−	s−	s−	s−	s−	s−	e	ℓ	ℓ	e	e	e	s	s	e	e	0	5+	0	2+
RH-500	s+	s+	s+	s+	s0	ℓ+	ℓ+	ℓ+	ℓ+	ℓ+	s	s	e	e	s	ℓ	ℓ	e	e	ℓ	5+	0	3+	0
H-850	s+	ℓ−	ℓ−	s+	ℓ−	ℓ+	s0	s0	ℓ+	ℓ+	s	s	e	s	s	ℓ	ℓ	e	ℓ	ℓ	2+	2+	4+	0
H-500	ℓ−	s−	s−	s−	s−	s−	ℓ−	ℓ−	ℓ−	ℓ−	s	s	s	s	s	ℓ	ℓ	ℓ	ℓ	ℓ	4+	1+	5+	0
H-250	s−	s−	s−	s−	s−	ℓ−	ℓ−	ℓ−	ℓ−	ℓ−	s	s	s	s	s	ℓ	ℓ	ℓ	ℓ	ℓ	5+	0	5+	0
T-850	s−	ℓ+	s−	s−	s−	ℓ−	s0	ℓ−	ℓ−	ℓ−	s	s	s	s	s	ℓ	ℓ	ℓ	ℓ	ℓ	4+	1+	5+	0
T-500	s−	s−	s−	s−	s−	ℓ−	ℓ−	ℓ−	ℓ−	ℓ−	s	s	s	s	s	ℓ	ℓ	ℓ	ℓ	ℓ	5+	0	5+	0
T-250	s−	s−	ℓ+	s−	ℓ+	ℓ−	ℓ−	s+	ℓ−	s+	s	s	s	s	s	ℓ	ℓ	ℓ	ℓ	ℓ	3+	2+	5+	0
																			total:		31+	12+	37+	2+

Both forecasts fail to predict the analysed intense circulation around the center of the low. Instead two low centers over the North Sea are predicted by both model versions. The mslp in the core of the cyclone in CBD is seen to be in best agreement with the analysis, which has a minimum value slightly above 992 hPa. The latter value is in good accordance with an observation-based subjective estimate of 991 hPa (Nielsen, 1997).

The conclusion based on the subjective evaluation of the cases presented in Figures 6 and 7 is that the CBD forecasts of msl pressure are in somewhat better agreement with the verifying CBC analysis than the corresponding CBC forecasts. There is no guarantee that this conclusion would hold for another selection of cases. However, it adds to the reliability of the conclusion that the selected cases represent all seasons and that each case contains one or more elements of extreme weather. Furthermore, it can be noted that the conclusion is in agreement with that drawn from the objective verification statistics presented in sections 3.1 and 3.2.

4. Sensitivity to the parameterization of moist processes

In this section results from three parallel experiments with different condensation/precipitation/evaporation parameterization schemes are intercompared. Two of the schemes (the Sundqvist scheme and the STRACO scheme) have cloud water as a prognostic variable, and contain parameterization of microphysical processes such as generation and evaporation of precipitation. In both schemes the generated net precipitation in each time step is assumed to fall out of the atmosphere. In contrast to the Sundqvist scheme the STRACO scheme contains a soft transition between the convective and stratiform regimes. Experiments have shown that the latter leads to a significant reduction of noise associated with abrupt switches between the convective and stratiform regimes. More information about the Sundqvist scheme is given in (Källén, 1996; Sundqvist et al., 1989; Sundqvist, 1993). More information about the STRACO scheme can be found in (Sass, 1997).

The third scheme is the Kuo/Cond scheme applied in the basic DMI-HIRLAM-G model. It does not contain cloud water as a diagnostic, or as a prognostic variable. The net condensation in each time step is assumed to fall out of the atmosphere as precipitation. In the convective (Kuo) part of the scheme a fraction of the condensate is used to moisten the convective cloud environments. The scheme contains a parameterization of evaporation of precipitation falling through cloud free layers. Further information about the Kuo/Cond scheme is given in (Källén, 1996).

4.1. Obs-verification

Averaged values of the obs-verification scores of CBD(kuo-eu) and CBE(sun-eu) are shown in Figures 8 to 11. It can be seen that the bias is best in the CBD forecasts for the following parameters: 2 m temperature, 850 hPa temperature, 500 hPa wind speed, and heights at 850 hPa and 250 hPa. The bias is best in the CBE forecasts for mslp, 250 hPa temperature and 850 hPa height. For the parameters not mentioned the bias is almost identical in the two model versions. It can be further noted that the temperature bias is systematically 'warmer' in CBD at the shown pressures, respectively representing the lower troposphere, the middle to upper troposphere, and the upper troposphere to lower stratosphere. The 'warmer' temperature bias in CBD is seen to be consistent with

a slower increase of the negative bias of the height field from 850 hPa to 250 hPa. It can also be noted that there is a more moderate cooling trend with forecast length in CBD, in particular at 850 hPa and 250 hPa. The initial numerical value of the bias of the height, temperature and wind speed can be considered as a measure of the quality of the analysis of the state of the free atmosphere. For some of the parameters the initial bias is substantial.

Concerning rms error the signal is more clear than for the bias. For all shown parameters except 850 hPa temperature and 850 hPa height the rms error is smallest in CBD, and for none of the parameters is the rms error smallest in CBE. Despite considerable variation with season and prevailing flow pattern the picture shown by the average scores generally holds for the individual periods as well (results not shown).

The differences in average values of the obs-verification scores for CBD(kuo-eu) and CBJ(str-eu) are generally small, as shown by Figures 12 to 15.

The bias in CBJ is slightly better for mslp, 250 hPa height and wind speed at 850 hPa and 250 hPa, while it is better in CBD for 500 hPa height, and temperature at 850 hPa and 500 hPa. For all other presented parameters the bias is similar in CBJ and CBD. The rms error is slightly smaller in CBJ for mslp, temperature at 850 hPa and 250 hPa and wind speed at 850 hPa, and it is slightly larger in CBJ for heights at 500 hPa and 250 hPa and for wind speed at 250 hPa.

The conclusions based on the obs-verification results in Figure 8 to 15 are that CBD(kuo-eu) performs somewhat better than CBE(sun-eu), while the quality of CBD and CBJ(str-eu) are similar.

The bias scores for height and temperature at the shown pressures indicate that the vertical diabatic heating rate profiles produced by the release of latent heat associated with precipitation are different in the three condensation schemes. It is indicated by the scores that the diabatic heating rate in the lower and upper troposphere is largest in CBD(kuo-eu) and CBJ(str-eu), respectively. In the middle troposphere the differences in heating rate are relatively small.

4.2. Field verification

The field verification results for CBD versus CBE and CBD versus CBJ are summarized in the two rightmost columns of Tables 4 and 5, respectively. According to these tables the bias scores in the inter-comparison of CBD(kuo-eu) and CBE(sun-eu) are best in CBD in 69% of the cases and best in CBE in only 27% of the cases. The corresponding numbers for the std. dev. error are 82% and 4%, respectively. Symbols applied in the tables are explained in section 3.2. In the inter-comparison of CBD(kuo-eu) and CBJ(str-eu) the bias is best in CBD in 48% of the cases and best in CBJ in 29% of the cases. The corresponding numbers for the std. dev. error are 49% and 24%, respectively.

From the field verification results in Tables 4 and 5 it can be concluded that CBD is clearly better than CBE, while CBD is somewhat better than CBJ. These conclusions are in agreement with those drawn from the obs-verification results in section 4.1, although the obs-verification scores were more alike, in particular for CBD and CBJ.

It can be noted from Table 5, columns 4 and 5, that the statistics for period P5 are outstanding in the sense that the std. dev. errors for CBJ are smaller than or equal to those for CBD. A similar picture is shown by the obs-verification scores for P5 (results

not shown). P5 was characterized by high frequency of deep convection over central and northern Europe. The smaller std. dev. errors in CBJ for this period therefore might indicate that the STRACO scheme simulates summer season deep convection better than the Kuo/Cond scheme.

An impression of the spatial variation of std. dev. error of mslp pressure is given in Figures 16 to 18. It is shown by Figures 16 and 17 that for P3 the std. dev. error of mslp in most of the integration domain is larger in CBE than in both CBD (Figure 16b) and CBJ (Figure 17b). The same also holds for the other periods (figures not shown). These results are seen to be in good agreement with the scores obtained for mslp in Tables 4 and 5.

It has been noted that CBJ has the best scores in P5 both in terms of obs-verification and field verification statistics. For mslp this is further indicated by the prevailing positive std. dev. error difference field (CBD minus CBJ) depicted in Figure 18b.

4.3. Case studies

The dates selected for the case studies are the same as in section 3.3. The autumn and winter case is shown in Figure 19. Shown are 48 hours forecasts of mslp for CBE(sun-eu) and CBJ(str-eu) together with the verifying CBE analyses.

The autumn case belongs to a group of 'high predictability' forecasts. It can be seen from Figure 19, left column, that the cyclone over the southeastern North Sea is best predicted by CBJ both with respect to shape and position. The predicted central mslp is about 979 hPa in CBE and about 977 hPa in CBJ. According to Figure 19 the analysed value in CBE is between 981 and 982 hPa, while an observation-based subjective estimate yields a value of 978 hPa. Accordingly, both model versions give a good prediction of the depth of the cyclone.

The winter case (Figure 19, right column) belongs to a group of 'low predictability' forecasts. In this case the CBE and CBJ forecasts of the intense cyclone over the Norwegian Sea are very different. The CBJ forecast is clearly in best agreement with the verifying CBE analysis, both with respect to depth, position and shape of the cyclone.

The spring and summer case shown in Figure 20 belongs to the 'high predictability' class of forecasts. In the spring case (Figure 20, left column) the position and depth of the filling low over the North Sea is somewhat better predicted by CBE, while the shape of the low is slightly better predicted in CBJ.

In the summer case (Figure 20, right column) both model versions predict a primary and secondary center in the cyclone over the North Sea, while the verifying CBE analysis as well as an observation-based subjective analysis has only one center with a mslp about 991 hPa (Nielsen, 1997). The subjective evaluation gives equal scores to CBE and CBJ.

A similar subjective evaluation of CBD in Figures 6 and 7 against CBJ in Figures 19 and 20 gives the result that CBD has the best score in P4 and CBJ the best score in P3. In P1 and P5 the scores are equal.

The subjective scores for the selected cases indicate that the CBJ forecasts generally are somewhat better than the CBE forecasts, and that the CBD and CBJ forecasts tend to be of equal quality. These conclusions are seen to be in good agreement with the conclusions based on the objective scores presented in sections 3.1, 3.2, 4.1 and 4.2.

Table 5: Kuo/Cond Euler contra STRACO Euler.

	CBD					CBJ					CBD					CBJ					Σ(bias)		Σ(std. dev.)	
param	bias scores					bias scores					std. dev. scores					std. dev. scores					D	J	D	J
period	P1	P2	P3	P4	P5	P1	P2	P3	P4	P5	P1	P2	P3	P4	P5	P1	P2	P3	P4	P5				
mslp	s+	ℓ−	ℓ−	s+	s+	ℓ+	s0	s0	ℓ+	ℓ+	s	ℓ	ℓ	e	ℓ	ℓ	s	s	e	s	3+	2+	1+	3+
RH-850	ℓ−	ℓ−	e−	e−	e−	s−	s−	e−	e−	e−	e	e	e	e	e	e	e	e	e	e	0	2+	0	0
RH-500	e+	e+	e+	e+	s0	e+	e+	e+	e+	ℓ+	s	s	s	s	e	ℓ	ℓ	ℓ	ℓ	e	1+	0	4+	0
H-850	s+	e−	ℓ−	ℓ+	ℓ−	ℓ+	e−	s−	s+	s0	s	e	ℓ	s	ℓ	ℓ	e	s	ℓ	s	1+	3+	2+	2+
H-500	s0	s−	s−	s−	s−	ℓ−	ℓ−	ℓ−	ℓ−	ℓ−	s	s	s	s	ℓ	ℓ	ℓ	ℓ	ℓ	s	5+	0	4+	1+
H-250	s−	e−	s−	ℓ−	s−	ℓ−	e−	ℓ−	s−	ℓ−	s	e	s	s	ℓ	ℓ	e	ℓ	ℓ	s	3+	1+	3+	1+
T-850	s−	ℓ+	s−	s−	s−	ℓ−	ℓ−	ℓ−	ℓ−	ℓ−	s	ℓ	s	e	ℓ	ℓ	s	ℓ	e	s	4+	1+	2+	2+
T-500	e−	ℓ−	s−	ℓ−	e−	e−	s−	ℓ−	s−	e−	e	e	s	s	ℓ	e	e	ℓ	ℓ	s	1+	2+	2+	1+
T-250	s−	s−	s+	ℓ−	ℓ+	ℓ−	ℓ−	ℓ+	s−	s+	s	s	s	s	ℓ	ℓ	ℓ	ℓ	ℓ	s	3+	2+	4+	1+
															total:						22+	13+	22+	11+

Table 6: Kuo/Cond Euler contra Kuo/Cond semi Lagrangian.

	CBD					CBF					CBD					CBF					Σ(bias)		Σ(std. dev.)	
param	bias scores					bias scores					std. dev. scores					std. dev. scores					D	F	D	F
period	P1	P2	P3	P4	P5	P1	P2	P3	P4	P5	P1	P2	P3	P4	P5	P1	P2	P3	P4	P5				
mslp	s+	ℓ−	ℓ−	s+	s+	ℓ+	s0	s0	ℓ+	ℓ+	s	s	s	s	s	ℓ	ℓ	ℓ	ℓ	ℓ	3+	2+	5+	0
RH-850	s−	e−	s−	s−	s−	ℓ−	e−	ℓ−	ℓ−	ℓ−	e	ℓ	ℓ	e	e	e	s	s	e	e	4+	0	0	2+
RH-500	ℓ+	s+	e+	e+	e0	s+	ℓ+	e+	e+	e0	s	s	s	s	s	ℓ	ℓ	ℓ	ℓ	ℓ	1+	1+	5+	0
H-850	s+	ℓ−	ℓ−	s+	ℓ−	ℓ+	s0	s0	ℓ+	ℓ+	s	s	s	s	s	ℓ	ℓ	ℓ	ℓ	ℓ	2+	2+	5+	0
H-500	e−	e−	e−	e0	s−	e−	e−	e−	e0	ℓ−	s	s	s	s	s	ℓ	ℓ	ℓ	ℓ	ℓ	1+	0	5+	0
H-250	s−	s−	s−	s−	s−	ℓ−	ℓ−	ℓ−	ℓ−	ℓ−	s	s	s	s	s	ℓ	ℓ	ℓ	ℓ	ℓ	5+	0	5+	0
T-850	s−	e+	ℓ−	e−	ℓ−	ℓ−	e+	s0	e−	s−	e	ℓ	ℓ	s	e	e	s	s	ℓ	e	1+	2+	1+	2+
T-500	s−	s−	s−	s−	s−	ℓ−	ℓ−	ℓ−	ℓ−	ℓ−	s	s	s	s	s	ℓ	ℓ	ℓ	ℓ	ℓ	5+	0	5+	0
T-250	e−	ℓ−	ℓ+	e−	s+	e−	s−	s+	e−	ℓ+	s	s	s	s	s	ℓ	ℓ	ℓ	ℓ	ℓ	1+	2+	5+	0
															total:						23+	9+	36+	4+

5. Eulerian versus semi-Lagrangian advection

In HIRLAM 3 a two time level semi-implicit and semi-Lagrangian advection scheme (McDonald and Haugen, 1993) was developed as an economical alternative to the Eulerian advection scheme. In this section results from the Eulerian experiments presented in section 4 are intercompared with corresponding semi-Lagrangian results. According to Table 2 the semi-Lagrangian experiments have been performed with sixth order implicit horizontal diffusion ($K = 10^{24}$) and with a time step three times longer than applied in the Eulerian experiments. This means that the extrapolation in time for each time step is $\Delta t_{\rm sl} = 720\,{\rm s}$ in the semi-Lagrangian runs and $2\Delta t_{\rm eu} = 480\,{\rm s}$ in the Eulerian runs. The semi-Lagrangian experiments corresponding to CBD, CBE and CBJ have been labeled CBF, CBG and CBK, respectively.

5.1. Obs-verification results

Obs-verification scores for CBD(kuo-eu) and CBF(kuo-sl) are shown in Figures 21 to 24. The shown scores are average values for the periods P1 to P5.

It can be seen that the bias is best in CBF for mslp, 2 m temperature, heights at 850 and 500 hPa and temperature at 250 hPa. In CBD the bias is best for height at 250 hPa, temperatures at 500 and 250 hPa and wind speeds at 850, 500 and 250 hPa. The std. dev. error is clearly smallest in CBD for most of the parameters shown. Only for 2 m-temperature is the std. dev. error smallest (and only marginally) in CBF.

It can be noted that the negative bias of the height field in CBF increases considerably faster upward through the troposphere than it does in CBD. It is for example shown in Figure 22 that at 48 hours forecast length the bias of the height field in CBF has dropped from -3 meters at 850 hPa to -20 meters at 250 hPa, while the corresponding drop in CBD only has been from -8 to -10 meters, with practically no change between 850 hPa and 500 hPa. The smaller negative bias of the 850 hPa height in CBF is consistent with a higher mslp bias (Figure 21), and the 'colder' bias of temperature in CBF at 500 hPa and 250 hPa, and its larger 'cooling' rate with forecast length, in particular at 500 hPa (Figure 23), is consistent with the variation of the height-field bias with pressure.

The results presented above are in good agreement with similar results obtained by (Gustafsson et al., 1996), for Swedish HIRLAM model versions with higher horizontal resolution ($0.2^\circ \times 0.2^\circ$) and lower vertical resolution (24 levels) than applied here.

Average obs-verification results for CBE(sun-eu), CBG(sun-sl), CBJ(str-eu) and CBK(str-sl) are shown in Figures 25 to 28. Note how similar the pattern shown by these figures is to that shown for CBD(kuo-eu) and CBF(kuo-sl) in Figures 21 to 24. It proves that a switch from Eulerian advection to semi-Lagrangian advection has almost the same effect on the obs-verification scores regardless of the type of parameterization of moist processes applied. In other words, the major contribution to the changes in obs-verification scores comes from the change in the treatment of dynamics. The contribution from the semi-Lagrangian response to changes in the parameterization of moist processes is only of secondary importance.

The conclusion that can be drawn from the results presented in Figures 21 to 28 are clear. In terms of rms errors the Eulerian forecasts have significantly better scores than the corresponding semi-Lagrangian forecasts. A major part of the differences in

bias scores between Eulerian and semi-Lagrangian experiments can be attributed to dynamic changes. Only a minor part can be attributed to a semi-Lagrangian response to changes in the parameterization of moist processes.

5.2. Field verification

The field verification scores for CBD(kuo-eu) versus CBF(kuo-sl), CBF(sun-eu) versus CBG(sun-sl) and CBJ(str-eu) versus CBK(str-sl) are presented in Tables 6, 7 and 8, respectively. The numbers in columns 6 and 7 of these tables show that the Eulerian model versions have the best scores both for bias and std. dev. error. For bias CBD is better than CBF in 51% of the cases, CBE is better than CBG in 69% of the cases and CBJ is better than CBK in 53% of the cases. The semi-Lagrangian versions CBF, CBG and CBK are best in respectively 20%, 9% and 13% of the cases. For std. dev. error CBD is better than CBF in 80% of the cases, CBE is better than CBG in 71% of the cases and CBJ is better than CBK in 73% of the cases. The semi-Lagrangian versions CBF, CBG and CBK are best in respectively 9%, 16% and 9% of the cases. The message from the field verification results in Tables 6 and 7 is that the Eulerian model versions in terms of field verification scores clearly perform better than the corresponding semi-Lagrangian versions. There is a high positive correlation between the obs-verification results and the field verification results, as seen for example by comparing obs-verification results for mslp, height and temperature in Figures 21 to 24 with the corresponding field verification scores in Table 6. For period P3 and a 48 hours forecast length the larger std. dev. error of mslp in the semi-Lagrangian forecasts are also shown by the difference fields CBF-CBD and CBK-CBJ in Figures 29b and 30b, respectively. A comparison of Figures 29a and 30a further shows that the std. dev. errors of mslp in the considered period tend to be slightly higher in CBF(kuo-sl) than in CBK(str-sl).

5.3. Case studies

Despite the better objective verification scores for the Eulerian forecasts the differences in mslp patterns in individual cases are often small. This is for example the case for the selected three pairs of 'high predictability' forecasts (autumn, spring and summer) shown in Figures 31 and 32 together with verifying CBJ(str-eu) analyses. The pair of forecasts shown is CBD (the Eulerian model version giving the overall best objective verification scores) and the corresponding semi-Lagrangian forecast CBF. In contrast, for the 'low predictability' case in Figure 31, right column, the semi-Lagrangian forecast CBF is of very poor quality.

6. Discussion

In discussions about the quality of a numerical weather prediction system, the focus often tends to be on the bias of the forecast minus observed (or analysed) mslp. It is shown by the present investigation that it can be misleading to put too much emphasis on the mslp bias. From a comprehensive number of objective and subjective scores it has been found that CBD (with Kuo/Cond, nonlocal vertical diffusion and Eulerian advection) is the best among the tested model versions, but evaluated from the mslp bias alone it is only number six (out of seven). The best models in terms of mslp bias are

Table 7: Sundqvist Euler contra Sundqvist semi-Lagrangian.

	CBE					CBG					CBE					CBG					Σ(bias)		Σ(std. dev.)	
param	bias scores					bias scores					std. dev. scores					std. dev. scores					E	G	E	G
period	P1	P2	P3	P4	P5	P1	P2	P3	P4	P5	P1	P2	P3	P4	P5	P1	P2	P3	P4	P5				
mslp	s+	s0	s0	s+	s+	ℓ+	ℓ+	ℓ+	ℓ+	ℓ+	s	s	s	s	s	ℓ	ℓ	ℓ	ℓ	ℓ	3+	0	5+	0
RH-850	s−	e−	s−	s−	s−	ℓ−	e−	ℓ−	ℓ−	ℓ−	ℓ	ℓ	ℓ	ℓ	ℓ	s	s	s	s	s	4+	0	0	5+
RH-500	s+	s+	e+	ℓ+	s+	ℓ+	ℓ+	e+	s+	ℓ+	s	e	e	s	e	ℓ	e	e	ℓ	e	3+	1+	2+	0
H-850	s+	s+	ℓ−	s+	s+	ℓ+	ℓ+	ℓ+	ℓ+	ℓ+	s	s	s	s	s	ℓ	ℓ	ℓ	ℓ	ℓ	4+	0	5+	0
H-500	s−	s−	e−	s−	s−	ℓ−	ℓ−	e−	ℓ−	ℓ−	s	s	s	s	e	ℓ	ℓ	ℓ	ℓ	e	4+	0	5+	0
H-250	s−	s−	s−	s−	s−	ℓ−	ℓ−	ℓ−	ℓ−	ℓ−	s	s	s	s	ℓ	ℓ	ℓ	ℓ	ℓ	s	5+	0	4+	1+
T-850	s−	s0	ℓ−	s−	e−	ℓ−	ℓ−	s−	ℓ−	e−	s	e	ℓ	e	ℓ	ℓ	e	s	e	s	2+	1+	1+	1+
T-500	s−	s−	s−	s−	s−	ℓ−	ℓ−	ℓ−	ℓ−	ℓ−	s	s	s	s	s	ℓ	ℓ	ℓ	ℓ	ℓ	5+	0	5+	0
T-250	ℓ−	ℓ−	e+	e−	s+	s−	s−	e+	e−	ℓ+	s	s	s	s	s	ℓ	ℓ	ℓ	ℓ	ℓ	1+	2+	5+	0
																				total:	31+	4+	32+	7+

Table 8: STRACO Euler contra STRACO semi-Lagrangian.

	CBJ					CBK					CBJ					CBK					Σ(bias)		Σ(std. dev.)	
param	bias scores					bias scores					std. dev. scores					std. dev. scores					J	K	J	K
period	P1	P2	P3	P4	P5	P1	P2	P3	P4	P5	P1	P2	P3	P4	P5	P1	P2	P3	P4	P5				
mslp	s+	s0	s0	s+	s+	ℓ+	ℓ+	ℓ+	ℓ+	ℓ+	s	s	s	s	s	ℓ	ℓ	ℓ	ℓ	ℓ	5+	0	5+	0
RH-850	e−	e−	s−	s−	s−	e−	e−	ℓ−	ℓ−	ℓ−	e	ℓ	ℓ	e	e	e	s	s	e	e	3+	0	0	2+
RH-500	ℓ+	e+	e+	e+	e+	s+	e+	e+	e+	e+	e	e	e	s	s	e	e	e	ℓ	ℓ	0	1+	2+	0
H-850	s+	ℓ−	ℓ−	s+	s0	ℓ+	ℓ+	s0	ℓ+	ℓ+	s	s	s	s	s	ℓ	ℓ	ℓ	ℓ	ℓ	3+	1+	5+	0
H-500	e−	ℓ−	e−	e−	s−	e−	s−	e−	e−	ℓ−	s	s	s	s	s	ℓ	ℓ	ℓ	ℓ	ℓ	1+	1+	5+	0
H-250	s−	s−	s−	s−	s−	ℓ−	ℓ−	ℓ−	ℓ−	ℓ−	s	s	s	s	s	ℓ	ℓ	ℓ	ℓ	ℓ	5+	0	5+	0
T-850	s−	e−	ℓ−	e−	s−	ℓ−	e−	s−	e−	ℓ−	e	e	ℓ	s	s	e	e	s	ℓ	ℓ	2+	1+	2+	1+
T-500	s−	s−	s−	s−	s−	ℓ−	ℓ−	ℓ−	ℓ−	ℓ−	s	s	s	s	s	ℓ	ℓ	ℓ	ℓ	ℓ	5+	0	5+	0
T-250	e−	ℓ−	ℓ+	e−	e+	e−	s−	s+	e−	e+	s	ℓ	s	s	s	ℓ	s	ℓ	ℓ	ℓ	0	2+	4+	1+
																				total:	24+	6+	33+	4+

CBE (with Sundqvist scheme, nonlocal vertical diffusion and Eulerian advection) and CBF (with Kuo/Cond, nonlocal vertical diffusion and semi-Lagrangian advection), but in terms of comprehensive scores they only rank as numbers four and six, respectively. With conservation of mass the mslp bias becomes a measure of the gain or loss of mass across the lateral boundaries of the model domain. The parallel experiments have shown that the mslp bias is quite sensitive to changes in both dynamics and physics. At a fixed forecast length a switch from Eulerian to semi-Lagrangian advection increases the mslp bias with an amount practically insensitive to changes in the parameterization of moist processes and turbulence. The results therefore show that semi-Lagrangian advection increases the net inflow of mass (relative to Eulerian advection) to the model domain by an amount which is practically independent of changes in the parameterization of moist processes and turbulence.

The semi-Lagrangian forecasts all have a large negative bias of the 250 hPa height, which is consistent with the significant negative temperature bias found in the middle troposphere. It can be noted that both the 250 hPa height bias and the 500 hPa temperature bias is more negative in the semi-Lagrangian experiments than in any of the Eulerian experiments. These results clearly demonstrate that an increase in the net inflow of mass is not the only effect of semi-Lagrangian advection. With this type of advection a significant cooling takes place in the middle troposphere.

The dynamic-thermodynamic response to a cooling source with a maximum in the middle troposphere is to lift the geopotential heights (and mslp if the penetration depth of the response is sufficiently large) below the source and to lower them above the source. The bias of temperature, height and mslp generated by the semi-Lagrangian advection does show a pattern similar to that described above. It is therefore suggested that the cooling source associated with semi-Lagrangian advection might originate from an inaccurate calculation of terms in the thermodynamic energy equation involving vertical velocity, most likely the energy conversion term.

It should be noted that for the response to occur the source must be localized not only in the vertical, but also in the horizontal directions. The latter will always be the case in a limited area model. For such a model the temperature bias at any level is an average over the model domain. Accordingly, any extremes in the vertical profile of temperature bias are localized horizontally by the model domain. Hence, it must be expected that the coupling to an external model in general alters the net mass flux across the lateral boundaries of the limited area model relative to the net mass flux into the same volume occurring in the external model itself.

Changes in the physical parameterization are in general expected to modify the model-domain-average of the vertical diabatic heating rate profile, or in terms of objective verification scores they are expected to modify the vertical profile of the temperature bias. If a change in the physical parameterization leads to a relative warming bias in a layer of the model atmosphere, the response in geopotential height would be a relative lowering and lifting below and above the layer, respectively. With a cooling bias the opposite would occur. It actually means that relative changes in the bias of mslp and pressure surface height in a qualitative way can be deduced from the relative changes in the temperature bias. The relationship for example appears as a significant negative correlation between relative changes in the bias of lower-tropospheric temperature and mslp. The corresponding correlation between changes in the bias of upper-tropospheric

temperature and mslp is expected to be weak due to a damping of the response with distance from the level of the extreme in temperature bias. Accordingly, the sensitivity of mslp bias to changes in the parameterization of turbulence and moist processes shown by the objective verification scores can be interpreted as a response (involving dynamic and thermodynamic interaction with the external model) to the variation in lower-tropospheric temperature bias generated by changes in the parameterization of subgrid-scale processes.

7. Conclusions

In the present report results from parallel tests of seven different versions of HIRLAM 2.5 have been presented. The performance of each model version has been evaluated in terms of objective verification scores and in terms of subjective estimates in selected cases. It has been found that CBD(kuo-eu) has the best scores, followed by CBJ(str-eu), CBC(kuo-local-eu), CBE(sun-eu), CBK(str-sl), CBF(kuo-sl) and CBG(sun-sl).

CBD is only marginally better than CBJ. In the summer period (P5), characterized by heavy convective precipitation in central and northern Europe, CBJ actually performs better than CBD. CBJ has a lower-tropospheric cold bias relative to CBD. Both models have a warm bias in the upper troposphere.

Replacement of local vertical diffusion (in CBC) with nonlocal vertical diffusion (in CBD) in combination with Kuo/Cond and Eulerian advection leads to a small improvement in verification scores. CBD has a lower-tropospheric warm bias relative to CBC.

The verification scores for the Eulerian model versions with Kuo/Cond and STRACO (CBD and CBJ, respectively) are clearly better than those for the model version with the Sundqvist scheme (CBE). CBJ has a lower-tropospheric cold bias and an upper-tropospheric warm bias relative to CBE.

It is notable that all model versions with semi-Lagrangian advection have poorer quality than their Eulerian counterparts. A significant cooling bias with a maximum in the middle troposphere seems to be the main reason for the poorer quality. It is suggested that the cooling source associated with semi-Lagrangian advection might originate from an inaccurate calculation of terms involving vertical velocity in the thermodynamical energy equation.

The results indicate that the bias of mslp in a limited area model is an inappropriate measure of model quality. The main reason seems to be that the mslp bias has a strong negative correlation with the lower-tropospheric temperature bias via a dynamic-thermodynamic coupling to the external model providing the boundary values. The problem is minimized if both models have identical physical parameterizations.

Appendix A. Specific features of DMI HIRLAM 2.5

a) Condensation and convection.

In the condensation scheme precipitation occurs at a threshold relative humidity of 100% (the code optionally allows for a smaller value). The specific latent energy parameter as function of temperature is cubic-shaped between the latent heat of evaporation at $0\,^{\circ}$C, and the latent heat heat of sublimation at $-15\,^{\circ}$C. (A discontinuous change of latent energy at $0\,^{\circ}$C applies to HIRLAM reference). In the convection scheme it is assumed that the specific humidity is well mixed during parcel lifting through the planetary

boundary layer. Above the unstable atmospheric boundary layer the air parcel is not affected by the influence of entrainment.

b) Cloud cover.
Cloud cover is parameterized as a function of relative humidity. As in the reference code the cloud cover CC is determined in every model level as a parabolic shaped function:

$$CC = \frac{(RH - RH_c)^2}{(1 - RH)^2}. \tag{1}$$

In (1) RH is the relative humidity, and RH_c is a threshold relative humidity

$$RH_c = \exp\left(-5.5\frac{\Delta p}{p}\right). \tag{2}$$

In (2), p is the pressure and Δp is the pressure increment between model half levels. The formula has been tuned to give approximately the same results as those of the reference model with the current vertical resolution (31 levels). In addition, it has the desired property that RH_c approaches 1 as the vertical resolution becomes infinitely high.

c) Vertical diffusion.
An asymptotic mixing length of 100 m is applied in the local first order vertical diffusion scheme. The corresponding value in the reference code is 300 m.

d) Horizontal diffusion.
Horizontal linear forth order diffusion is done along pressure surfaces for both humidity, temperature and wind components. In the reference system diffusion along pressure surfaces is done only for specific humidity.

References

Gustafsson, N., Meuller, L., and Tallsjö, A. (1996). A parallel test with semi-Lagrangian advection in the swedish HIRLAM. *Hirlam Newsletter* **23**, 11–20.

Holtslag, A. A. M. and Boville, B. A. (1993). Local versus nonlocal boundary layer diffusion in a global climate model. *J. Climate* **6**, 1825–1842.

Källén (1996). HIRLAM Documentation Manual. system 2.5. Technical report, SMHI, Norrköbing, Sweden.

Louis, J. F., Tiedtke, M., and Geleyn, J. F. (1981). A short history of the PBL parameterization at ECMWF. In *ECMWF Workshop on Boundary-Layer Parameterization*, pages 59–79, ECMWF.

McDonald, A. and Haugen, J.-E. (1993). A two time level, three-dimensional, semi-lagrangian and semi-implicit grid point model. II. extension to hybrid coordinates. *Mon. Wea. Rew.* **121**, 2077–2087.

Nielsen, N. (1997). Tordenstormen over København den 30. juni 1997. *Vejret* **73**, 1–14.

Nielsen, N. W. and Sass, B. H. (1995). Recent work at DMI on vertical diffusion. *Hirlam Newsletter* **22**, 17–28.

Sass, B. H. (1997). Reduction of numerical noise connected to the parameterization of cloud and condensation processes in the HIRLAM model. *Hirlam Newsletter* **29**, 37–45.

Sundqvist, H. (1993). Inclusion of ice phase of hydrometers in cloud parameterization for mesoscale and large-scale models. *Beitr. Phys. Atmosph.* **66**, 137–147.

Sundqvist, H., Berge, E., and Kristiansson, J. E. (1989). Condensation and cloud parameterization studies with a mesoscale numerical weather prediction model. *Mon. Wea. Rew.* **117**, 1641–1657.

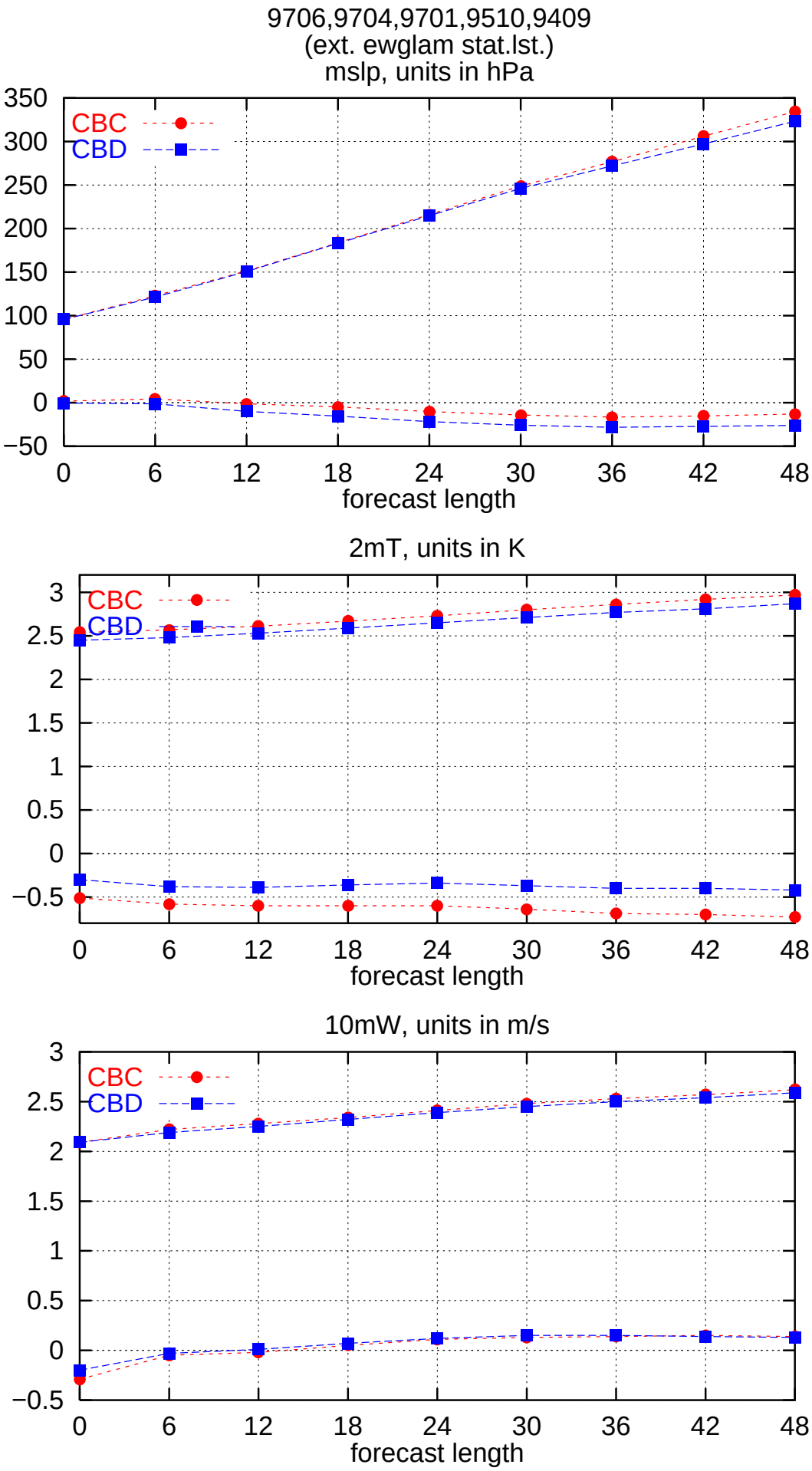

Figure 1: Obs verification of surface parameters for local (CBC) versus nonlocal (CBD) vertical diffusion experiment.

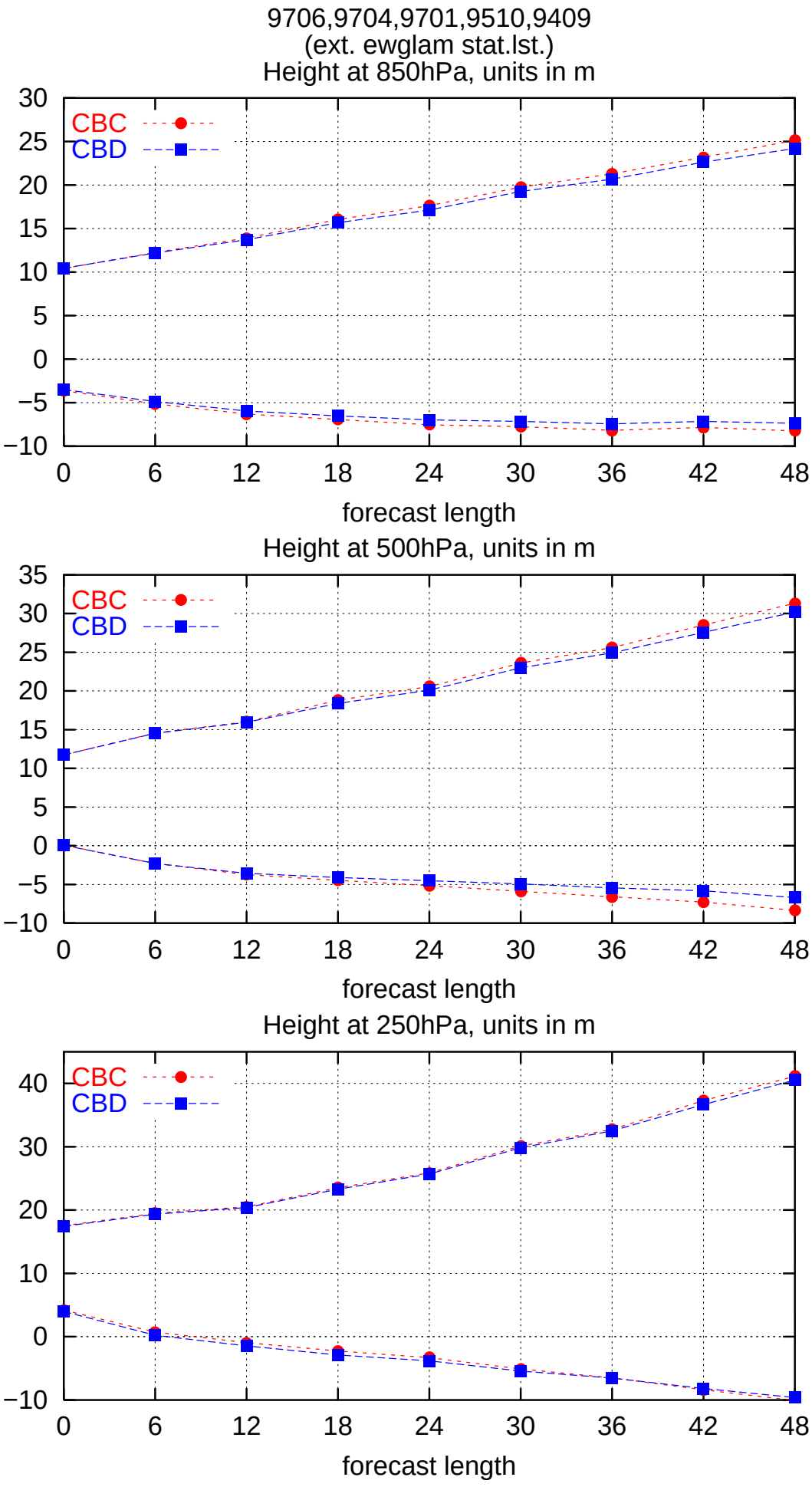

Figure 2: Obs verification of geopotential height at 850, 500 and 250 hPa level for local (CBC) versus nonlocal (CBD) vertical diffusion experiment.

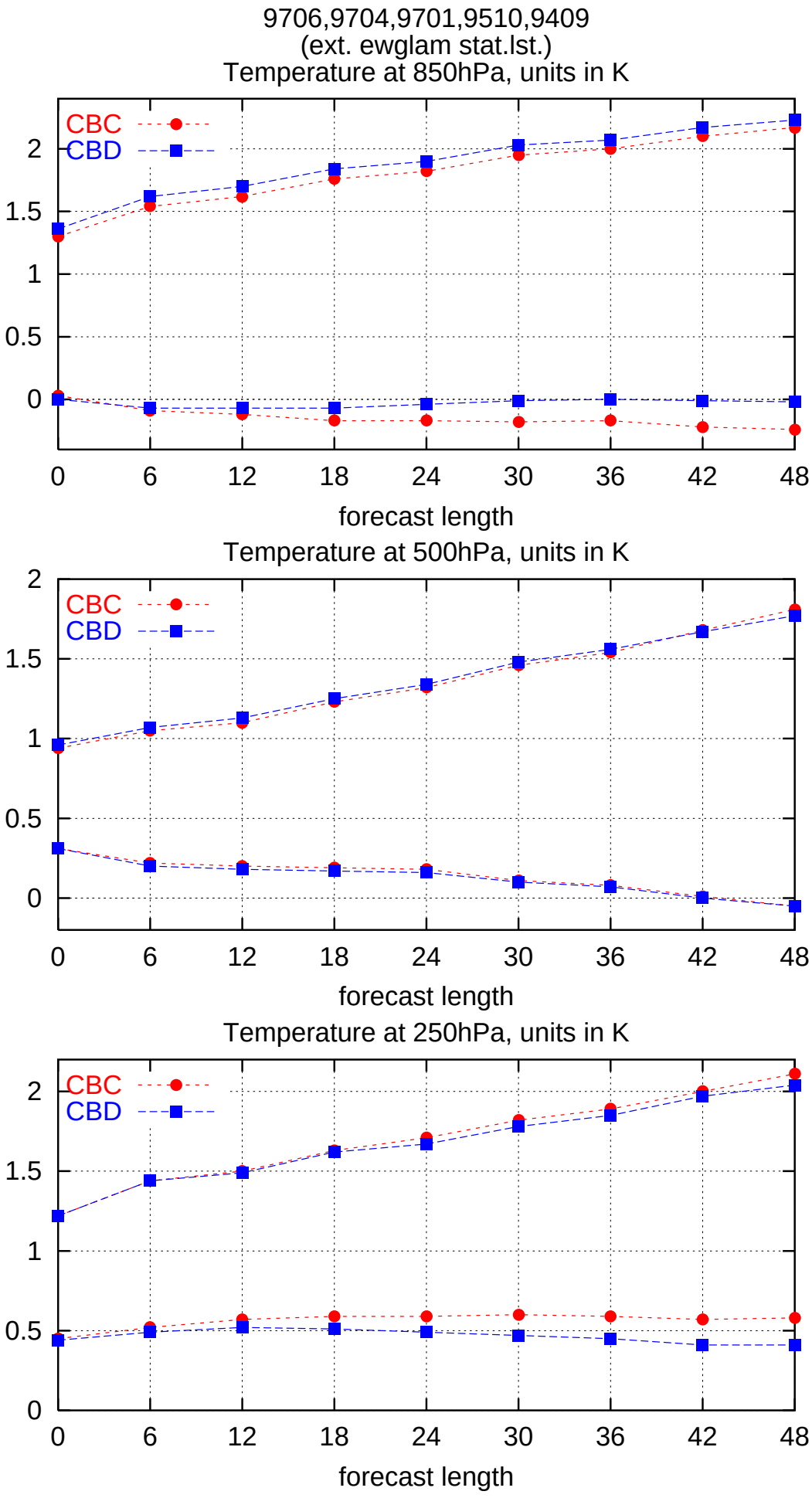

Figure 3: Obs verification of temperature at 850, 500 and 250 hPa level for local (CBC) versus nonlocal (CBD) vertical diffusion experiment.

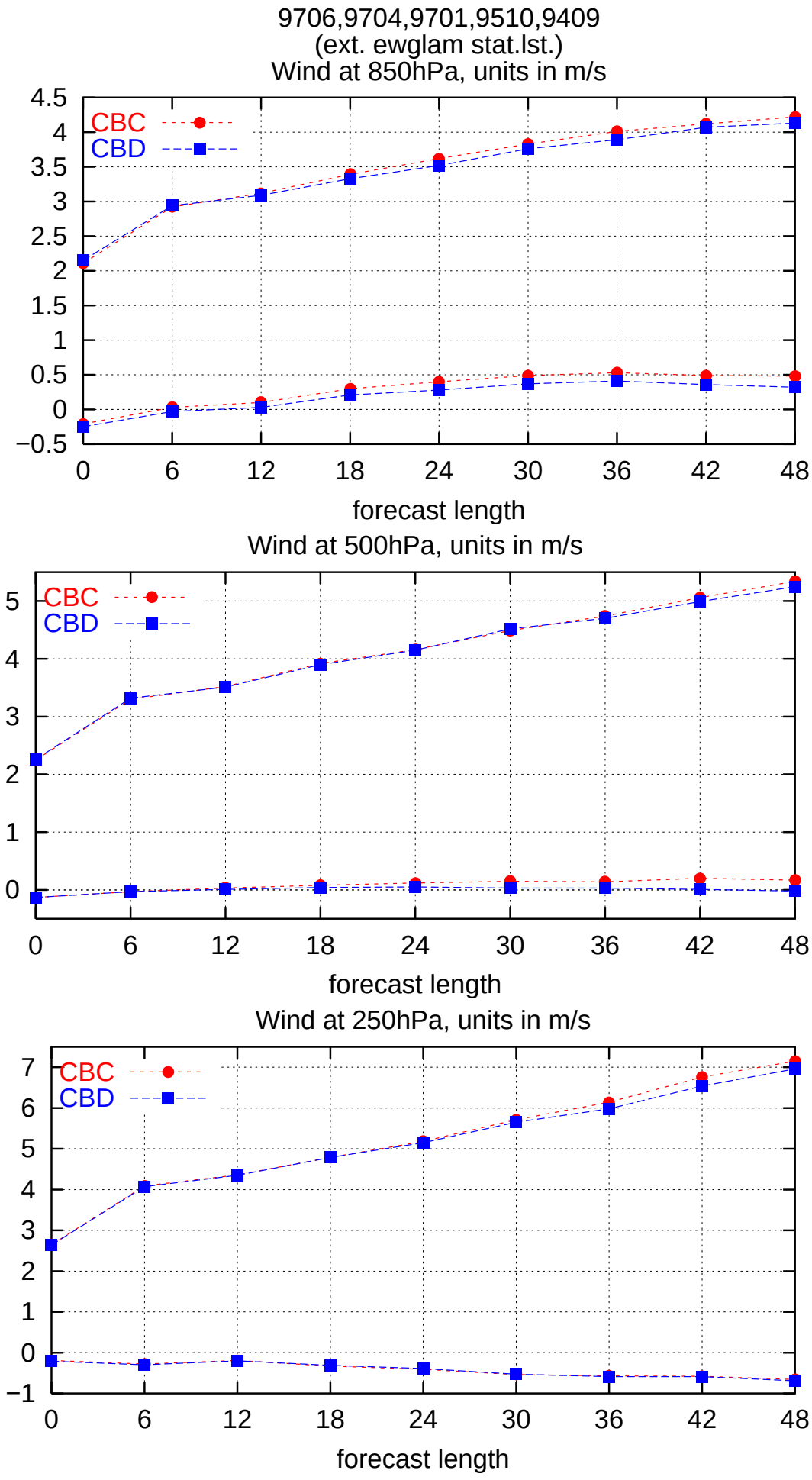

Figure 4: Obs verification of wind at 850, 500 and 250 hPa level for local (CBC) versus nonlocal (CBD) vertical diffusion experiment.

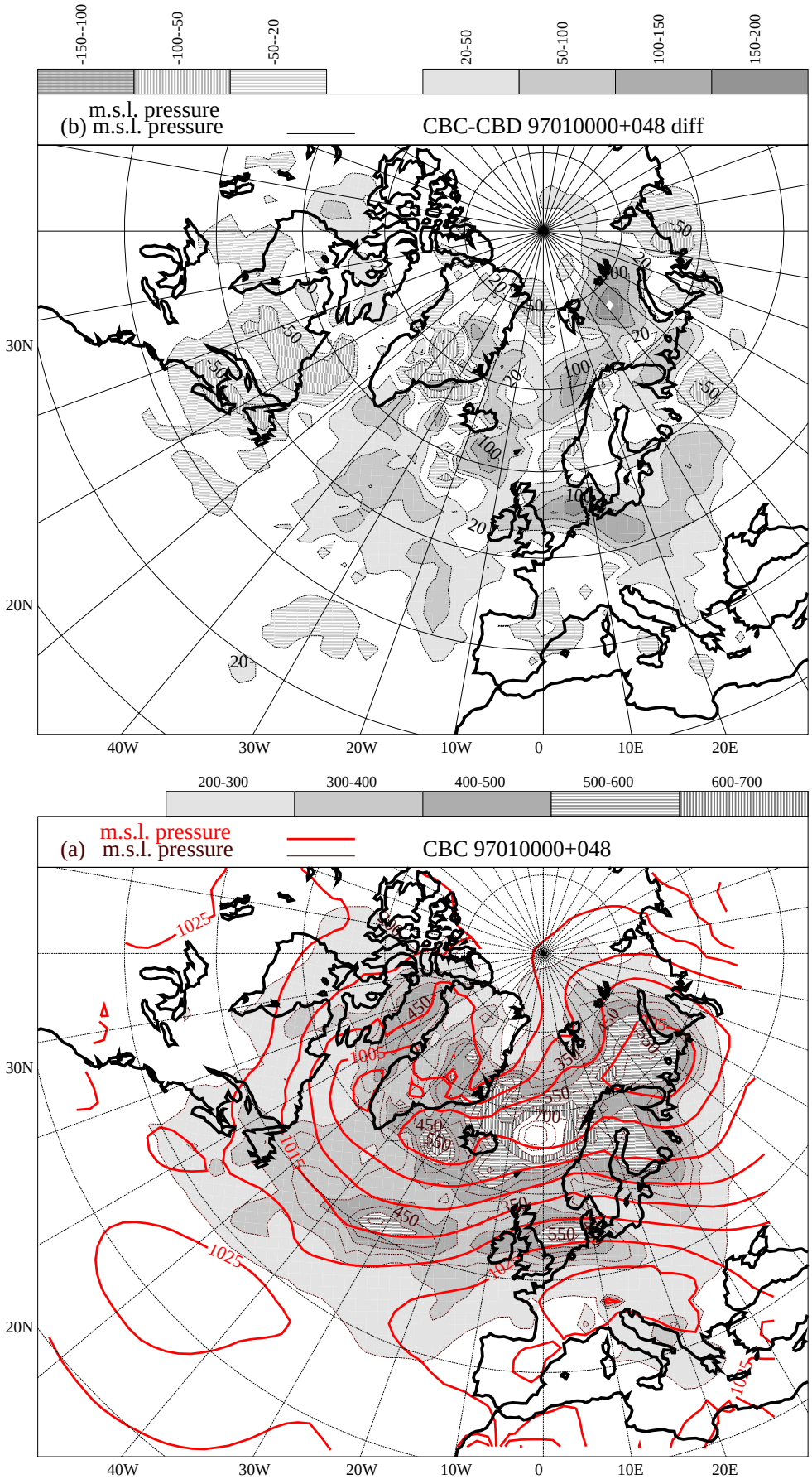

Figure 5: **(a)** Average mslp together with the std. dev. error of mslp for CBC in period P3. **(b)** For the same period the difference in std. dev. error of mslp between local (CBC) and non-local (CBD) first order diffusion.

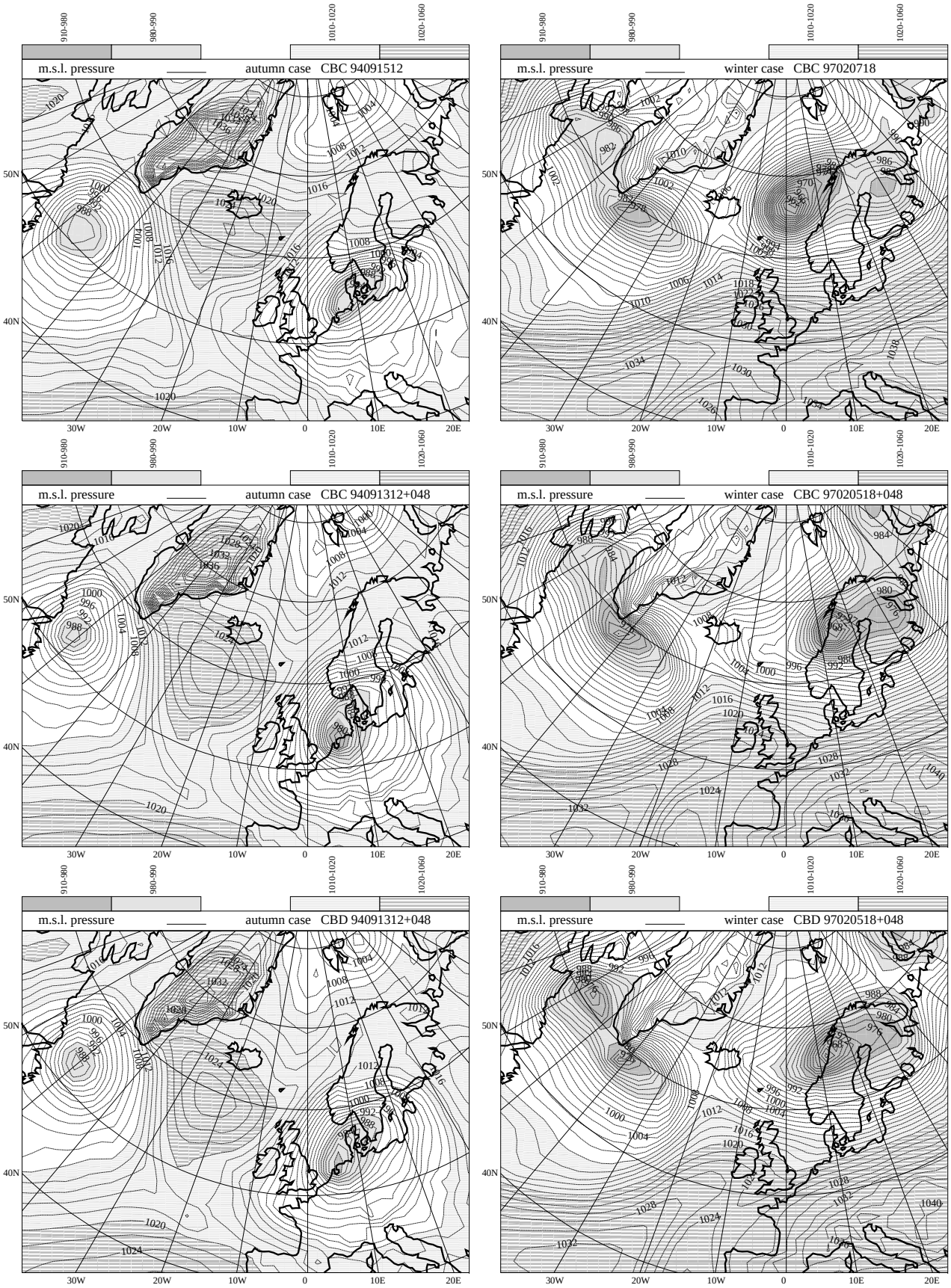

Figure 6: Autumn and winter case is for model versions with non-local (CBD) and local (CBC) first order diffusion. Shown are 48 hours forecasts together with the CBC verifying analyses.

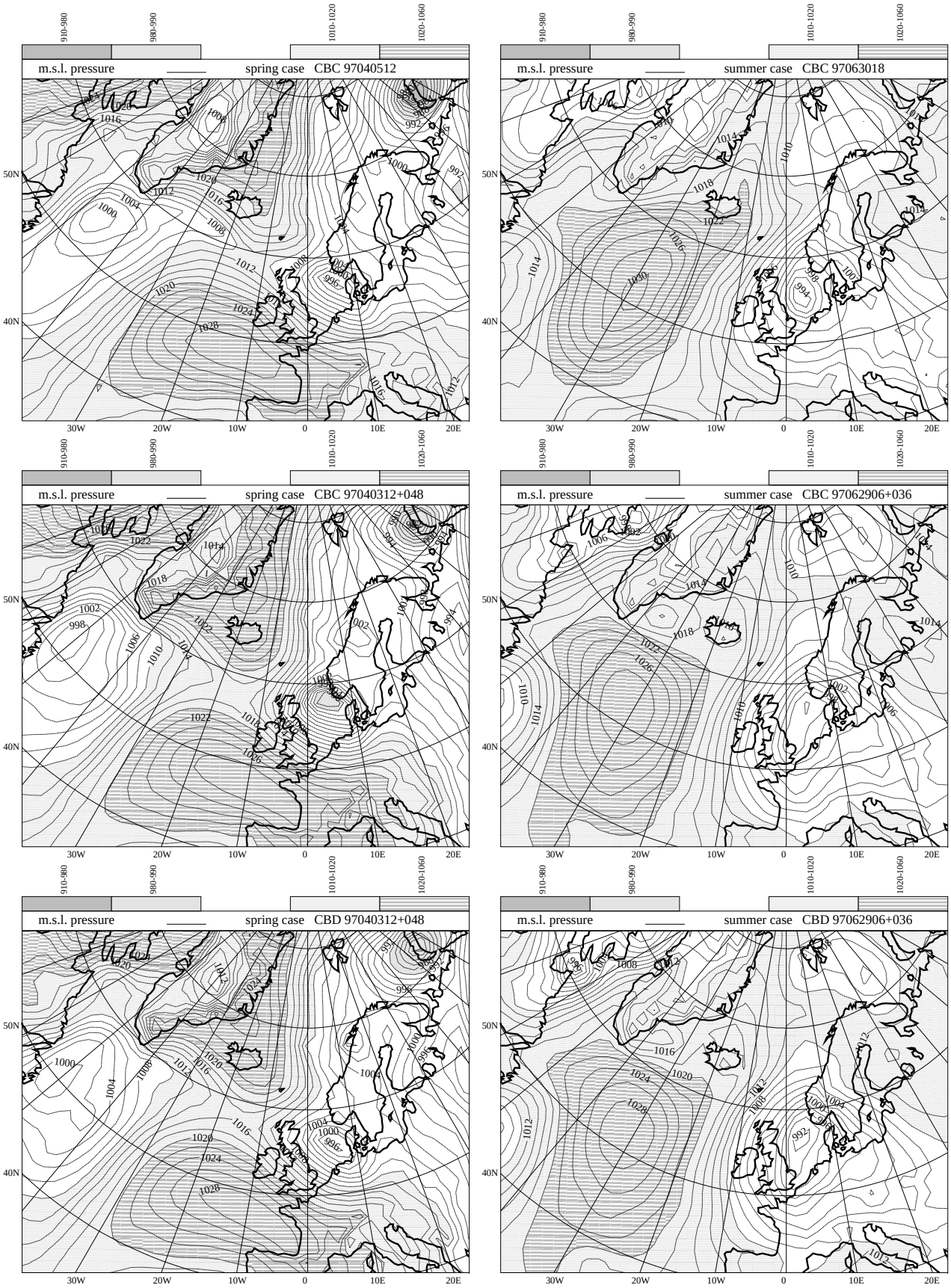

Figure 7: Spring and summer case is for model versions with non-local (CBD) and local (CBC) first order diffusion. Shown are 48 hours forecasts (spring case) and 36 hours forecasts (summer case) together with the CBC verifying analyses.

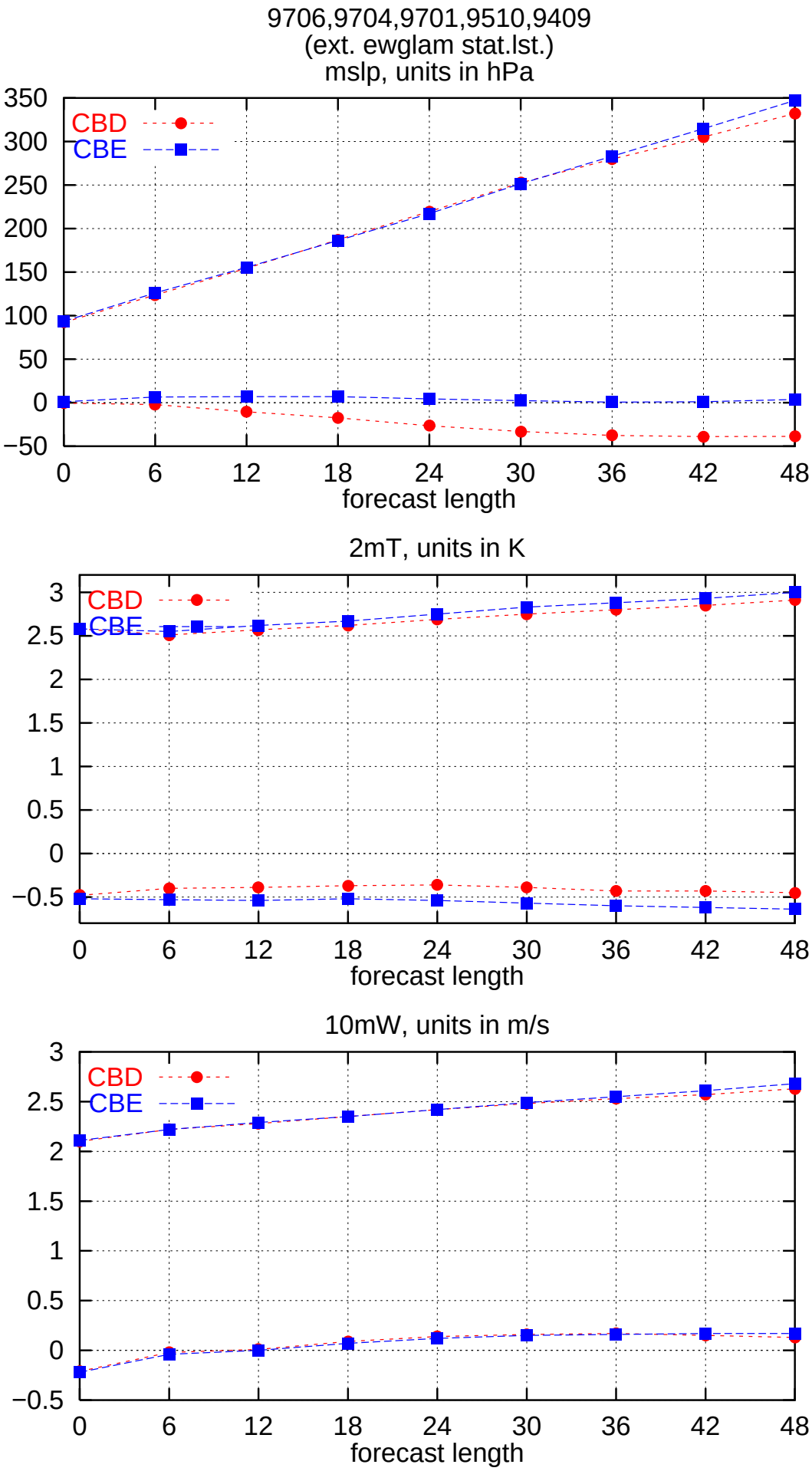

Figure 8: Obs verification of surface parameters for Kuo/Cond Euler (CBD) versus Sundqvist Euler (CBE).

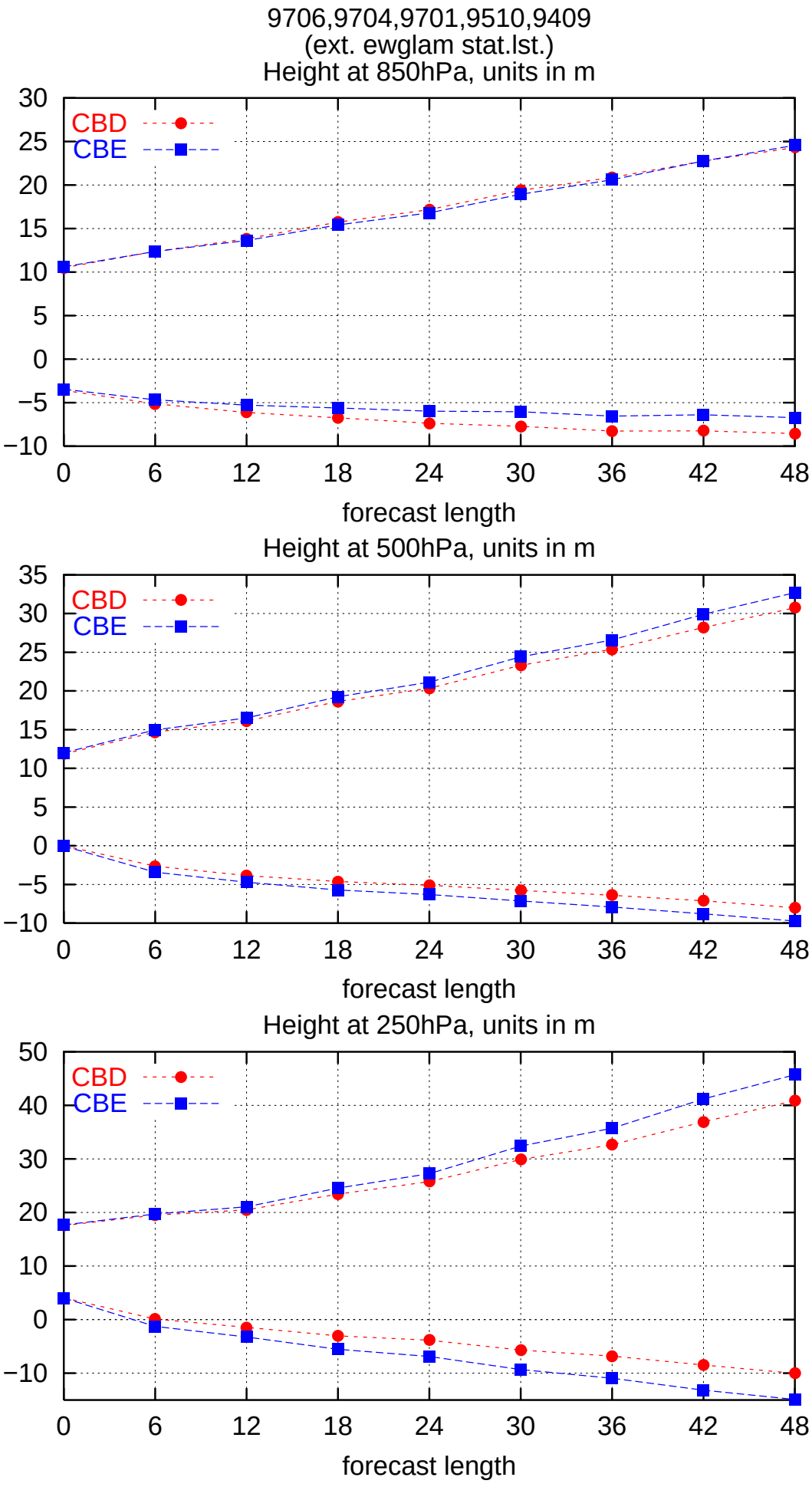

Figure 9: Obs verification of geopotential height at 850, 500 and 250 hPa level for Kuo/Cond Euler (CBD) versus Sundqvist Euler (CBE).

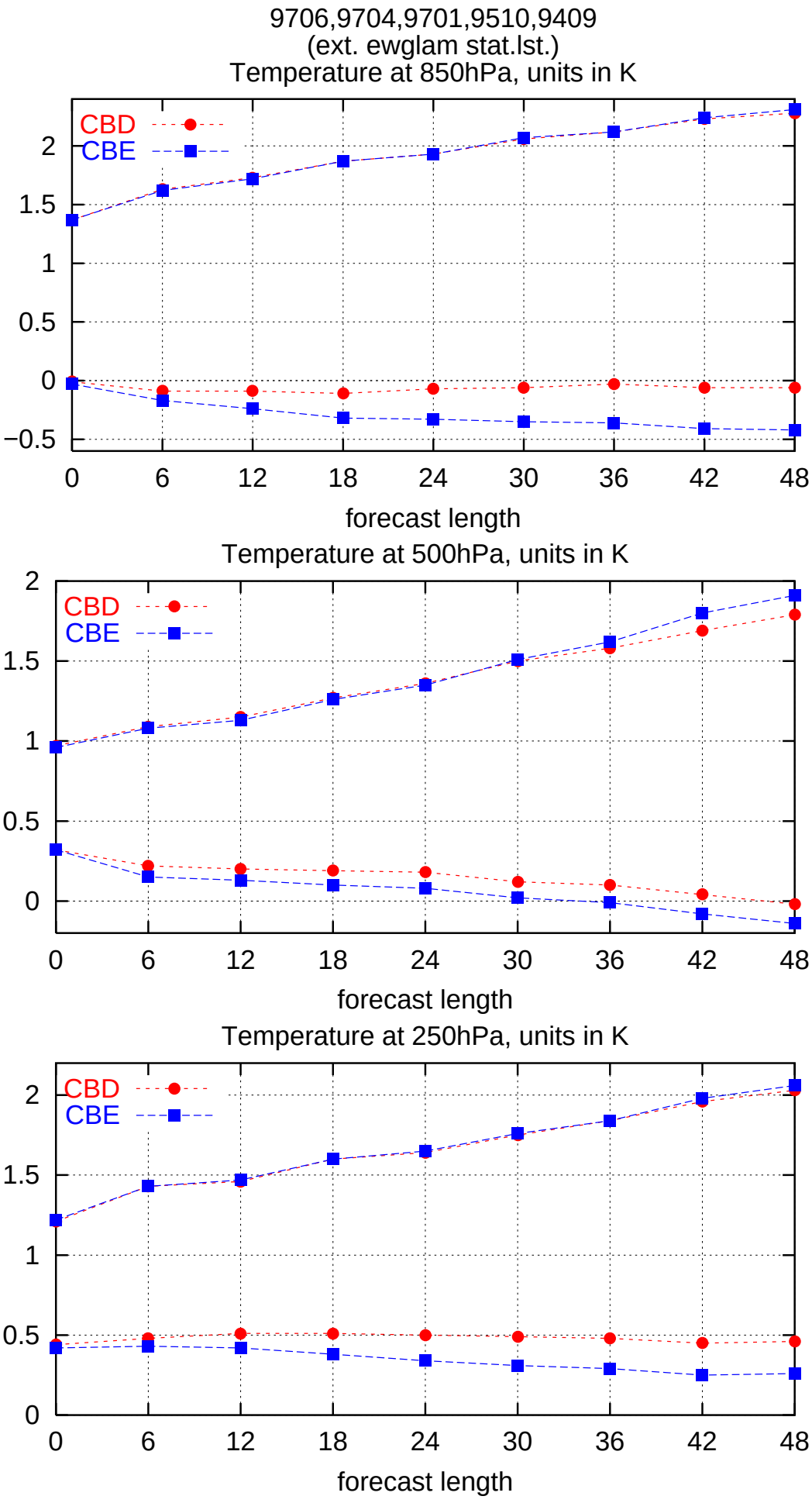

Figure 10: Obs verification of temperature at 850, 500 and 250 hPa level for Kuo/Cond Euler (CBD) versus Sundqvist Euler (CBE).

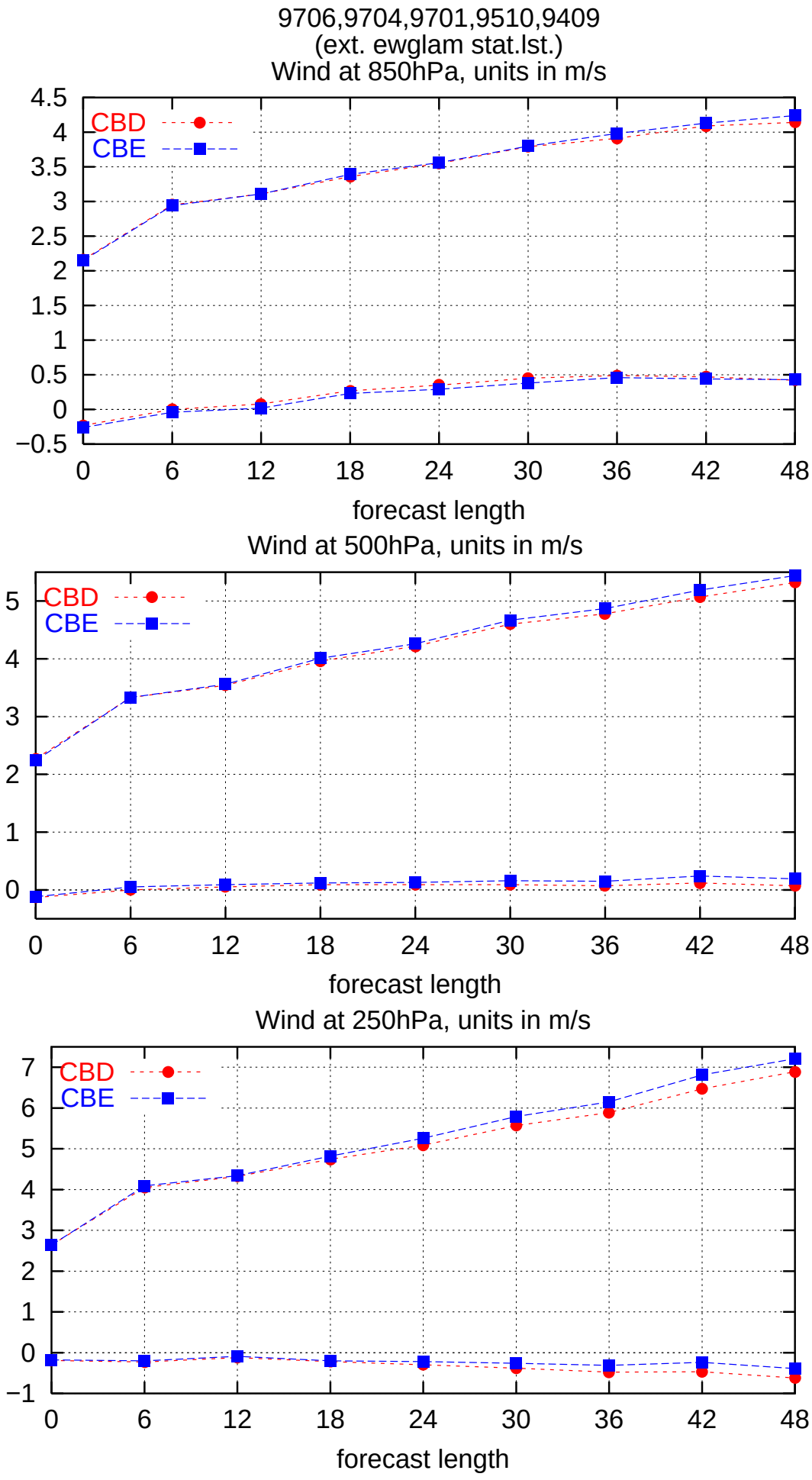

Figure 11: Obs verification of wind at 850, 500 and 250 hPa level for Kuo/Cond Euler (CBD) versus Sundqvist Euler (CBE).

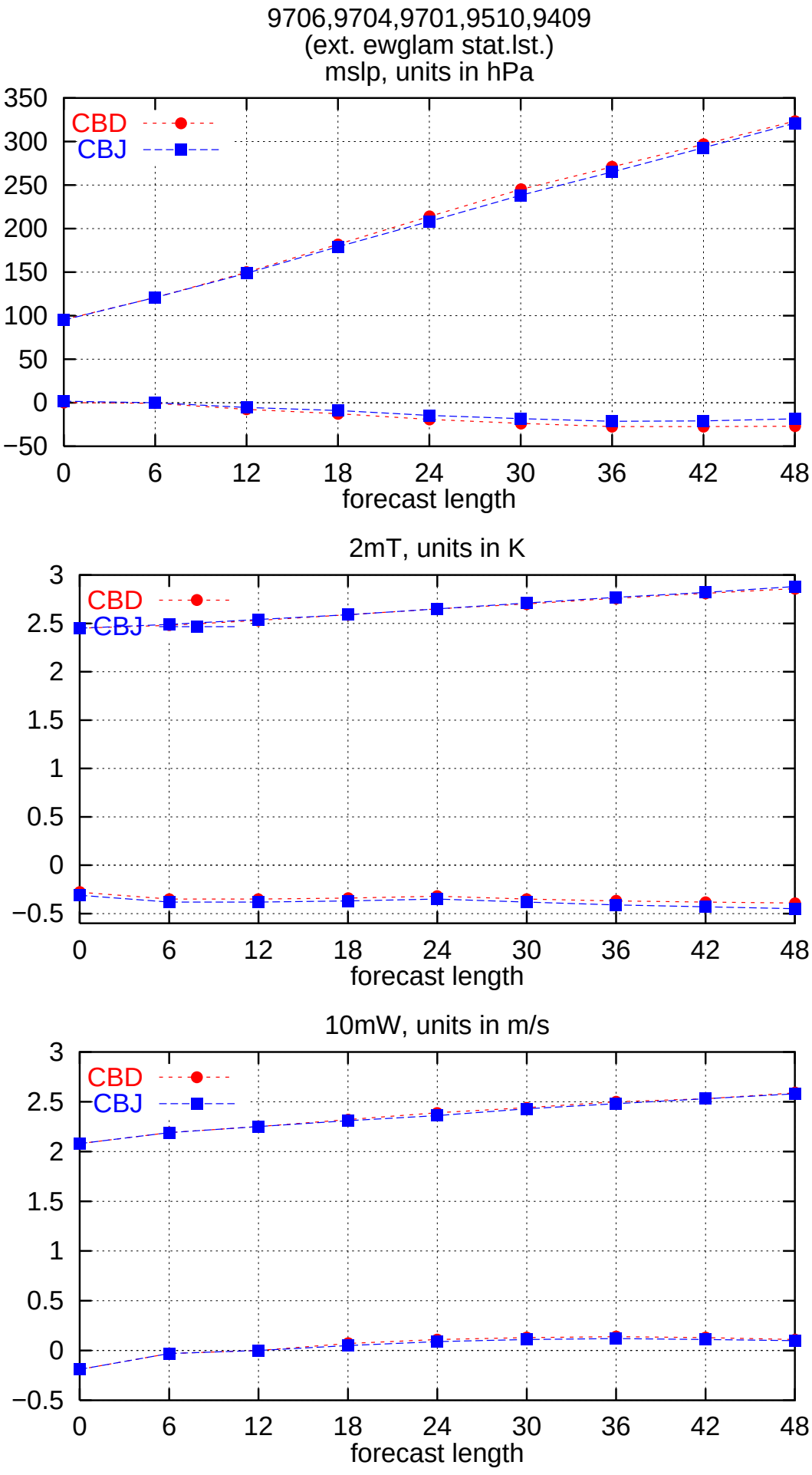

Figure 12: Obs verification of surface parameters for Kuo/Cond Euler (CBD) versus STRACO Euler (CBJ).

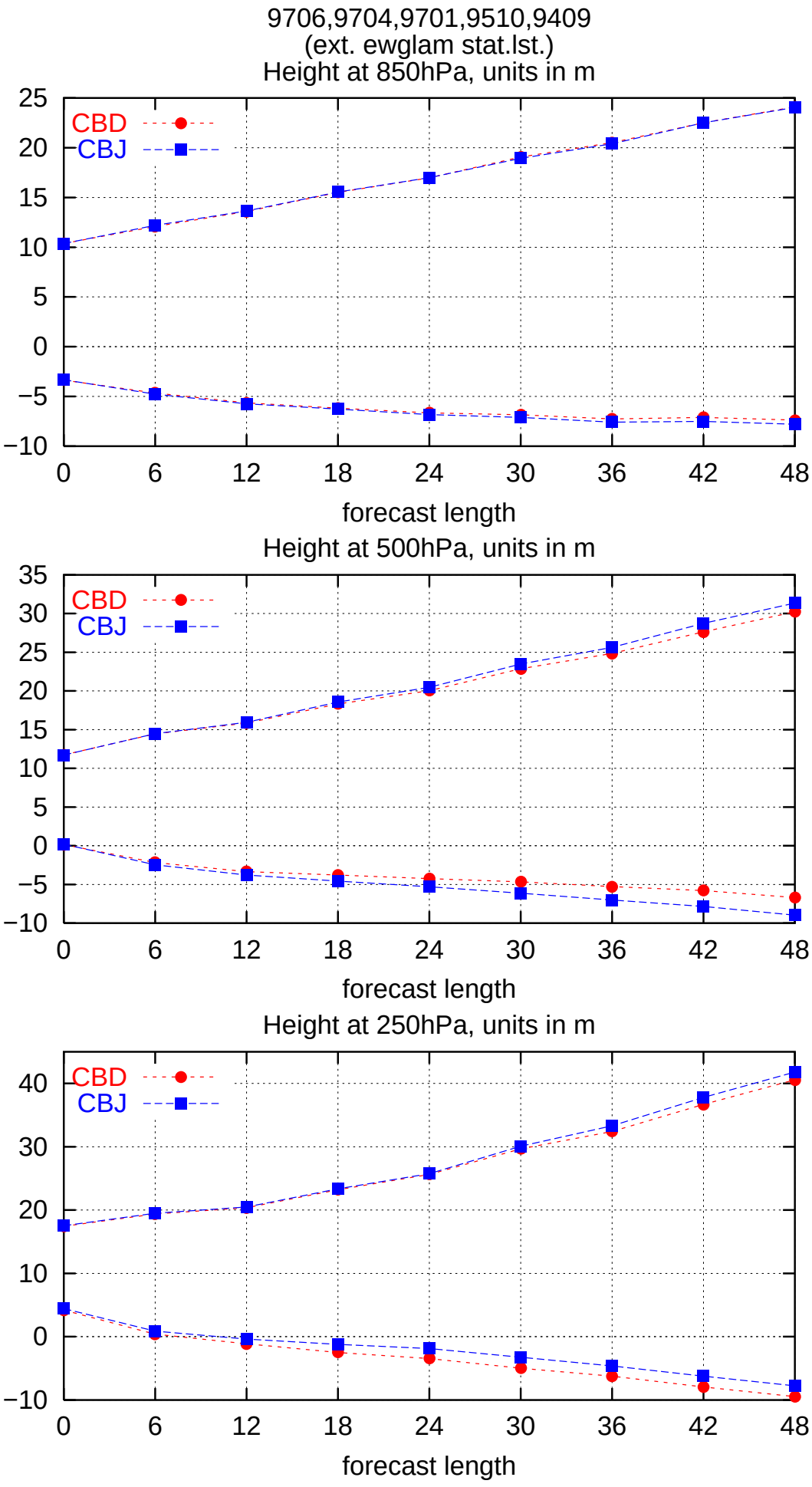

Figure 13: Obs verification of geopotential height at 850, 500 and 250 hPa level for Kuo/Cond Euler (CBD) versus STRACO Euler (CBJ).

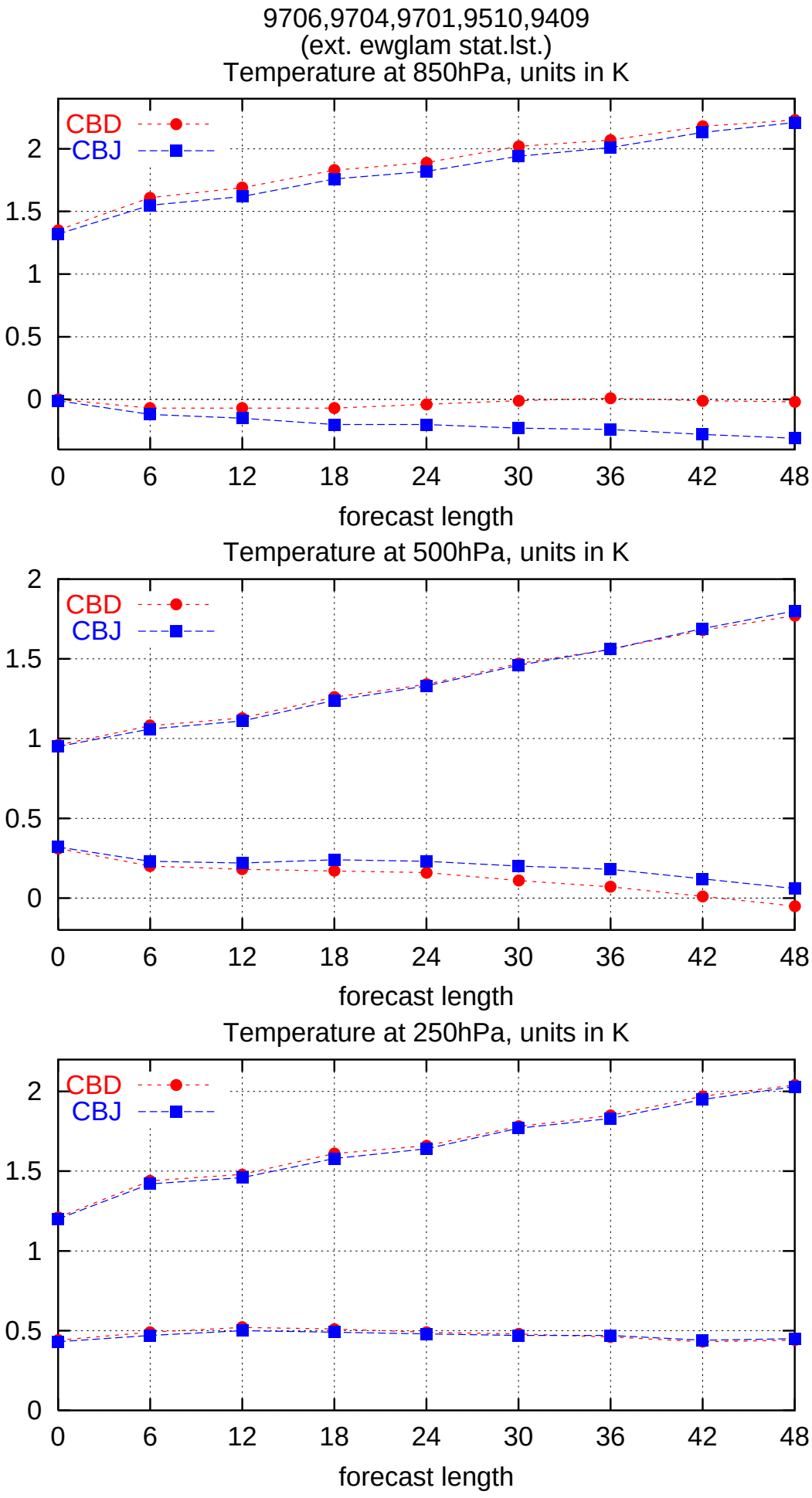

Figure 14: Obs verification of temperature at 850, 500 and 250 hPa level for Kuo/Cond Euler (CBD) versus STRACO Euler (CBJ).

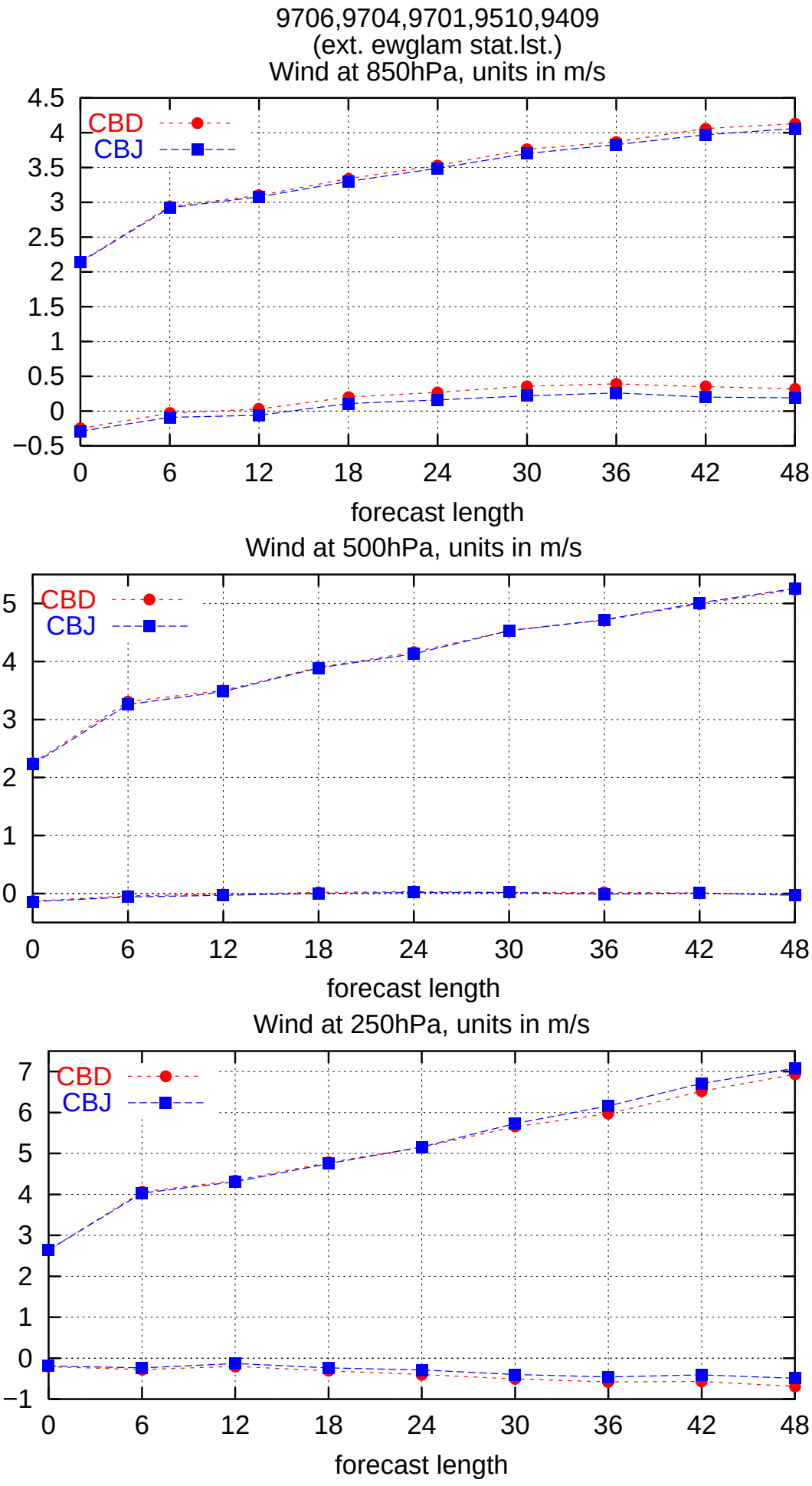

Figure 15: Obs verification of wind at 850, 500 and 250 hPa level for Kuo/Cond Euler (CBD) versus STRACO Euler (CBJ).

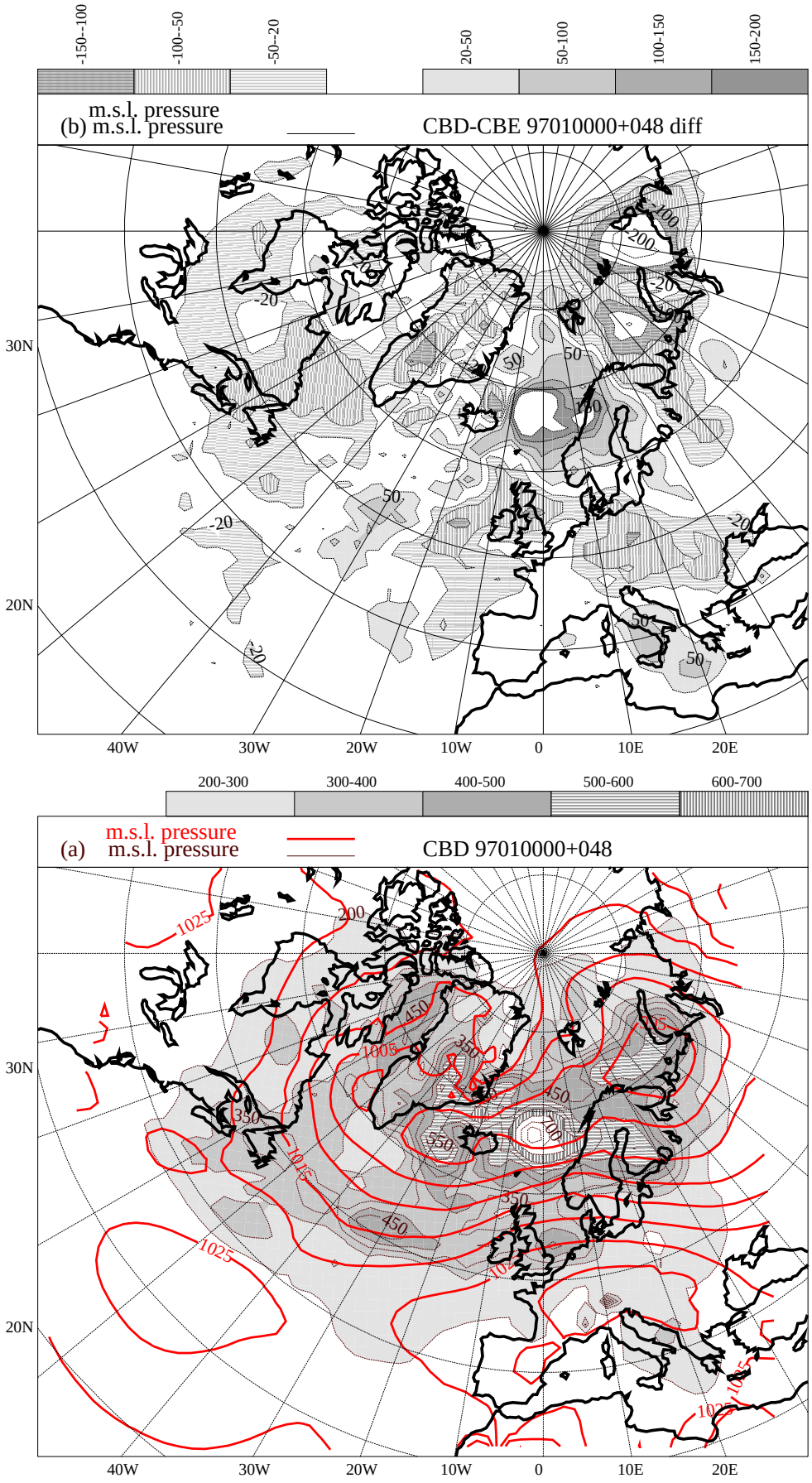

Figure 16: **(a)** Average mslp together with the std. dev. error of mslp for CBD in period P3. **(b)** For the same period the difference in the std. dev. of mslp between Kuo/Cond Euler (CBD) and Sundqvist Euler (CBE).

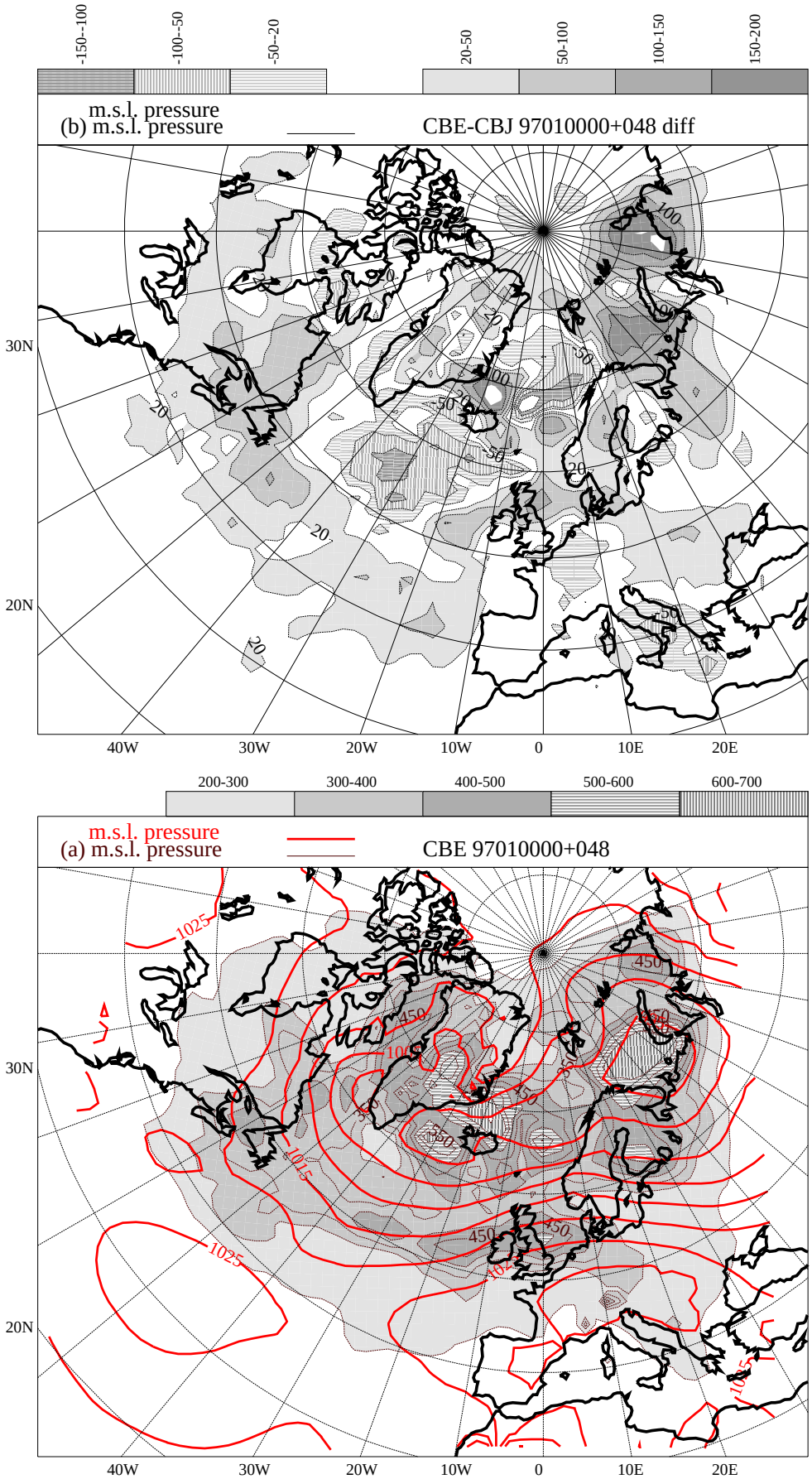

Figure 17: **(a)** Average mslp together with the std. dev. error of mslp for CBE in period P3. **(b)** For the same period the difference in the std. dev. of mslp between Sundqvist Euler (CBE) and STRACO Euler (CBJ).

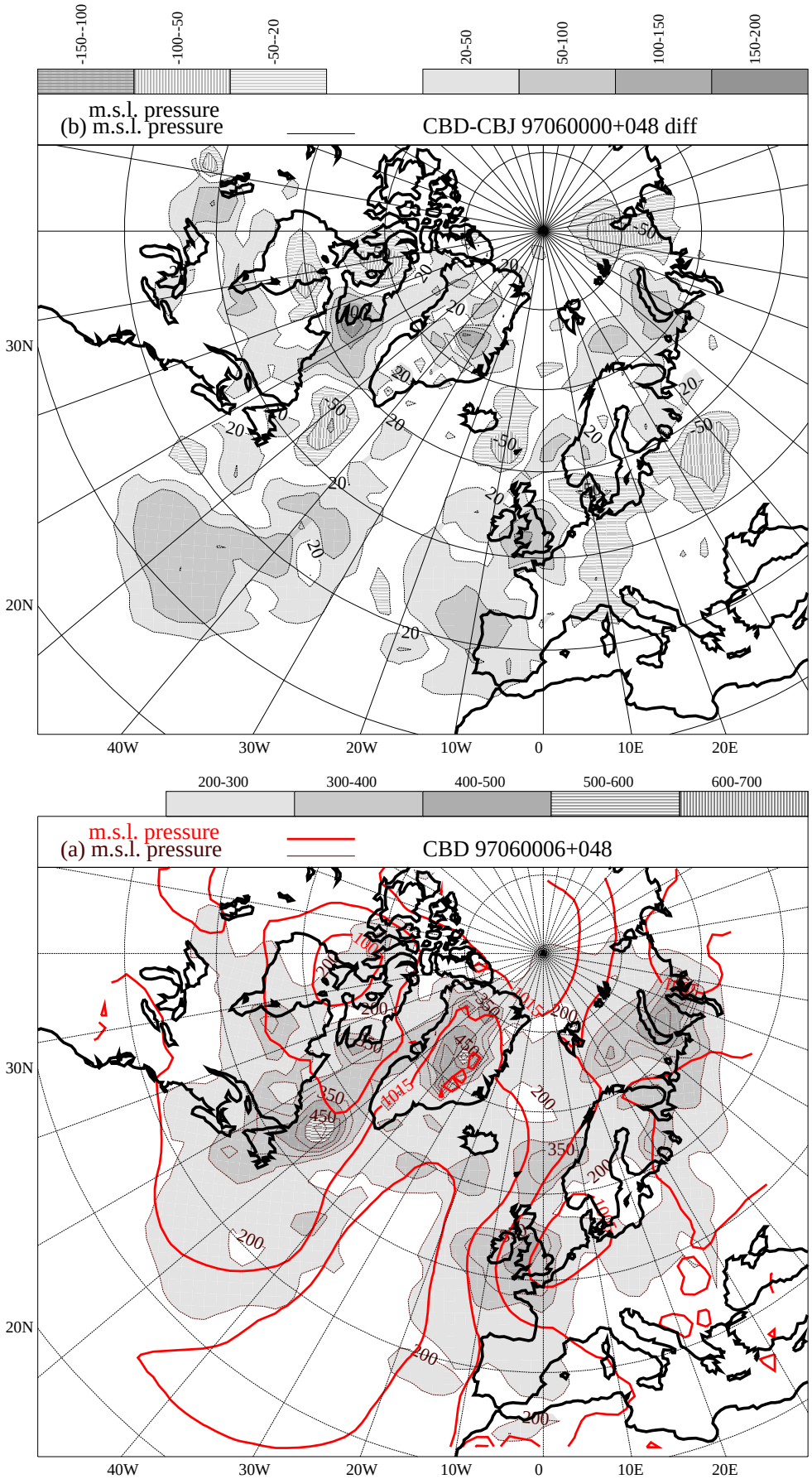

Figure 18: **(a)** Average mslp together with the std. dev. error of mslp for CBD in period P5. **(b)** For the same period the difference in the std. dev. of mslp between Kuo/Cond Euler (CBD) and STRACO Euler (CBJ).

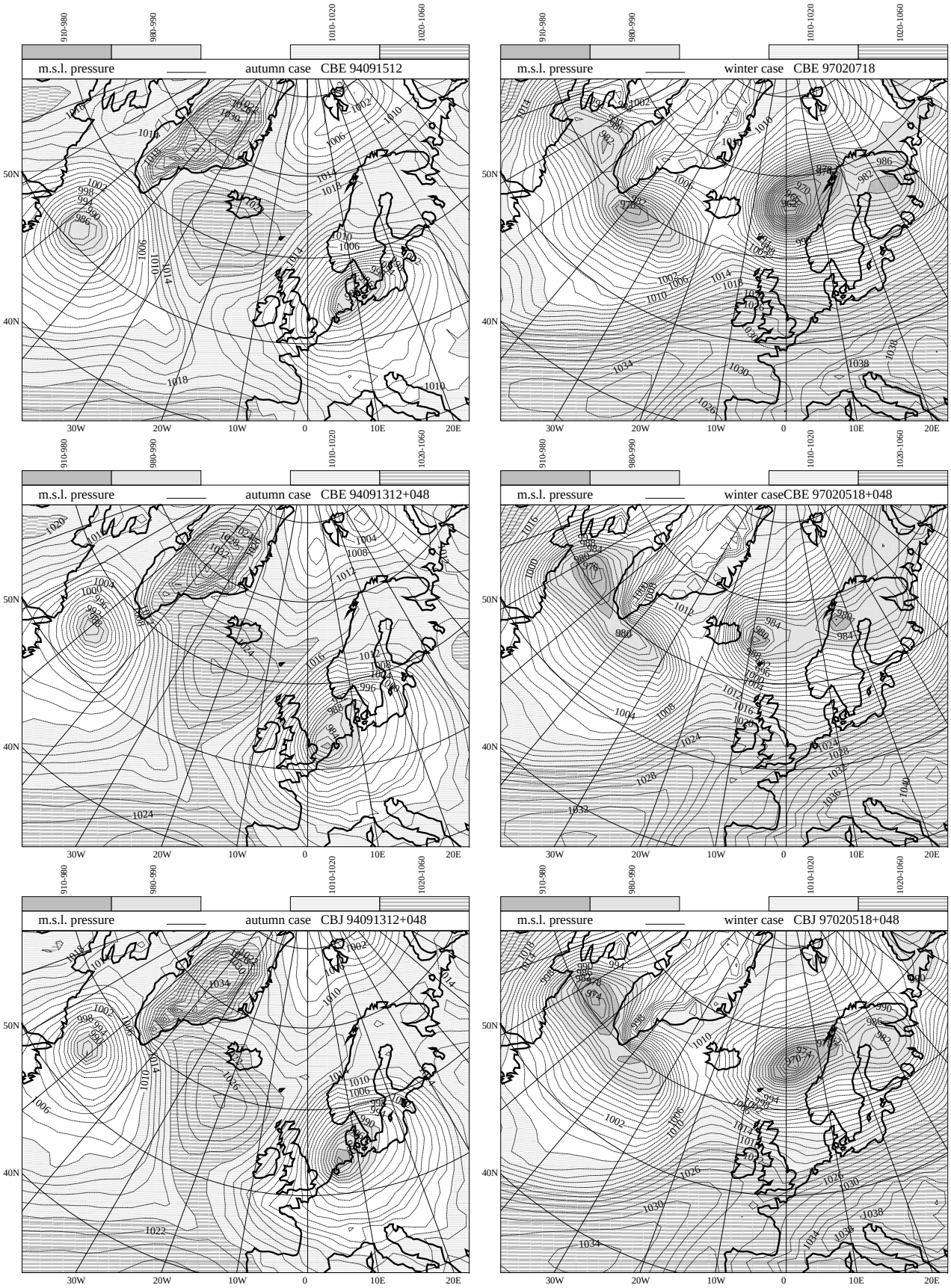

Figure 19: Autumn and winter case is for model versions with Sundqvist Euler (CBE) and STRACO Euler (CBJ). Shown are 48 hours forecasts together with the CBE verifying analyses.

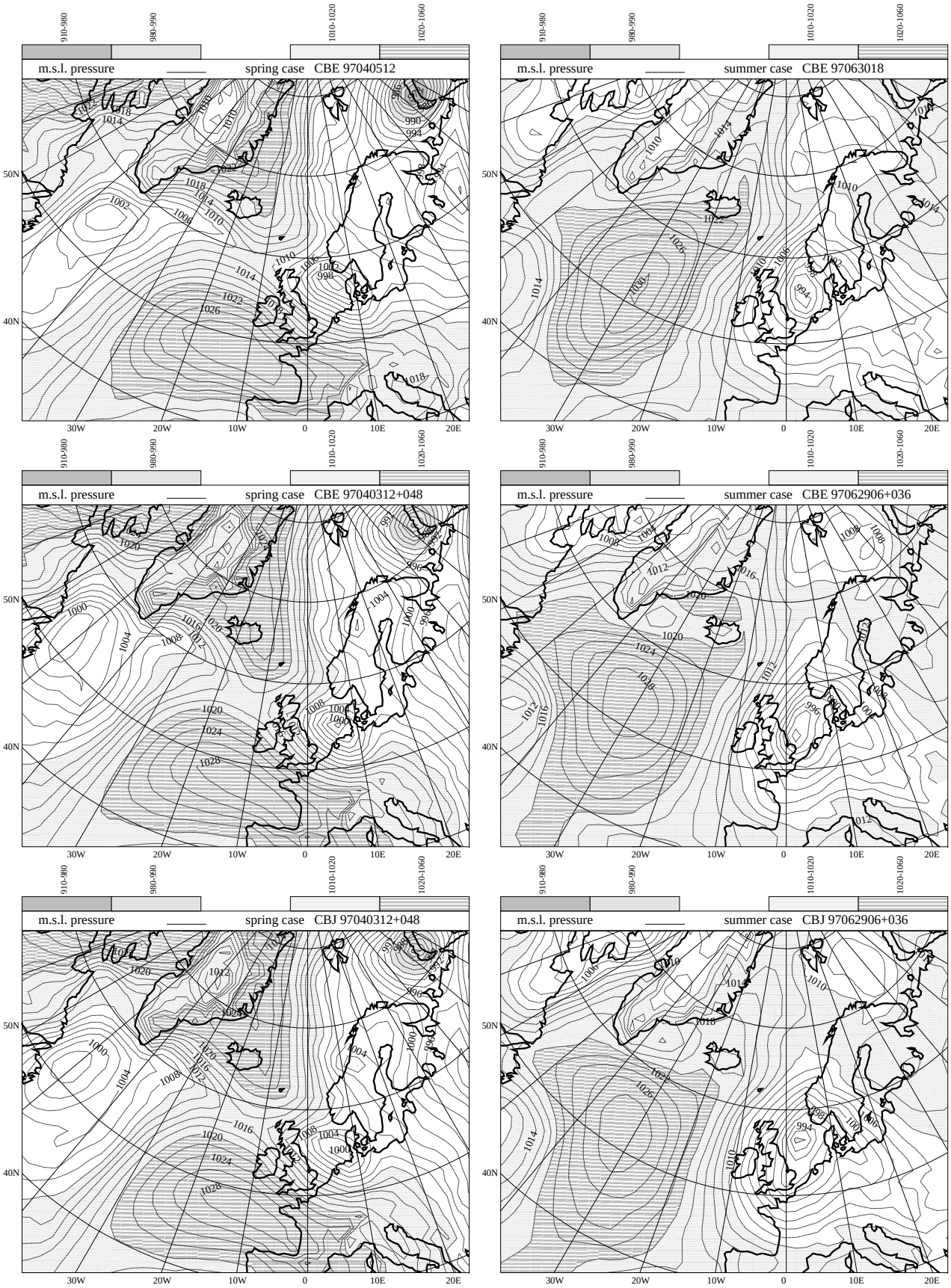

Figure 20: Spring and summer case is for model versions with Sundqvist Euler (CBE) and STRACO Euler (CBJ). Shown are 48 hours forecasts (spring case) and 36 hours forecasts (summer case) together with the CBE verifying analyses.

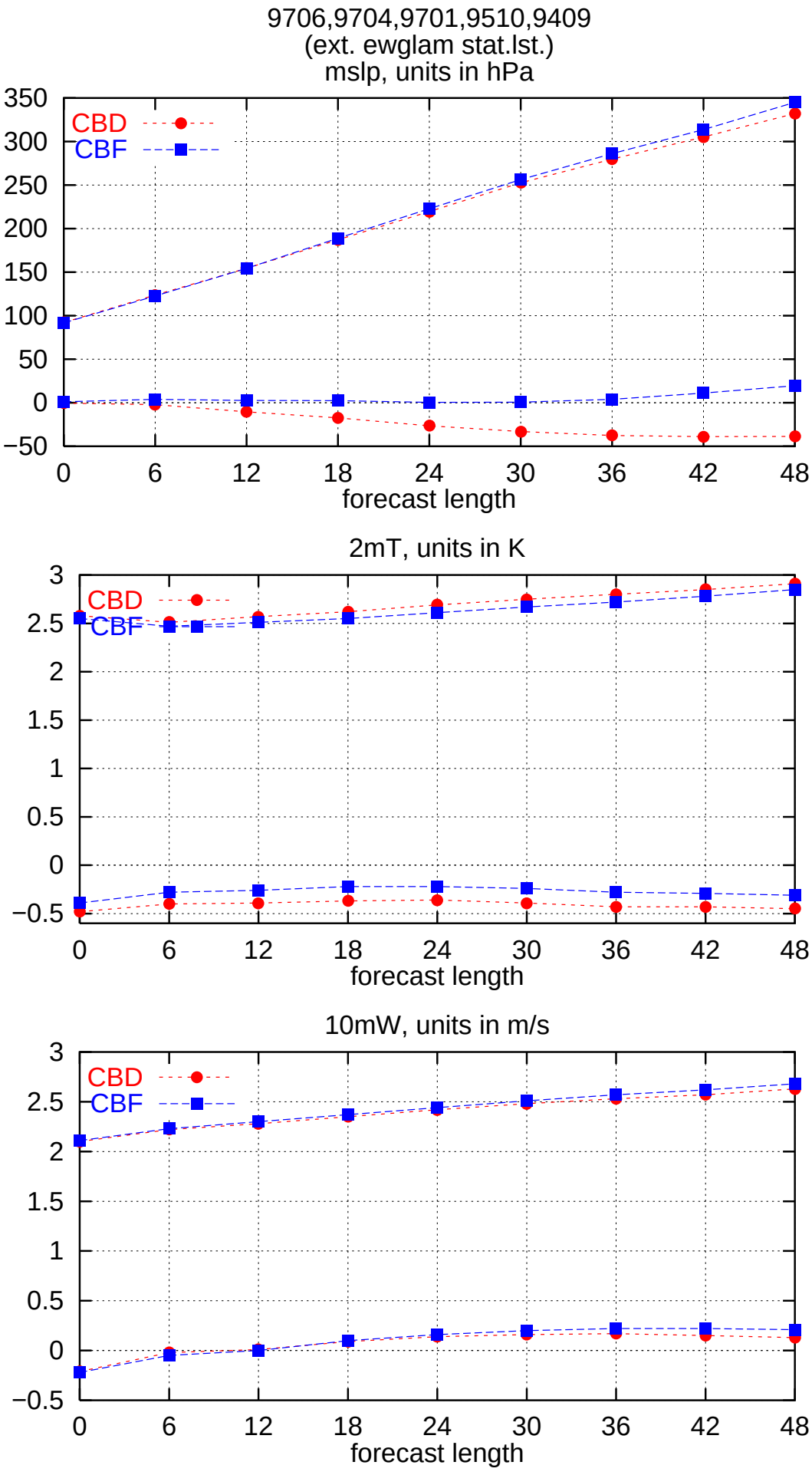

Figure 21: Obs verification of surface parameters for Kuo/Cond Euler (CBD) versus Kuo/Cond semi-Lagrangian (CBF).

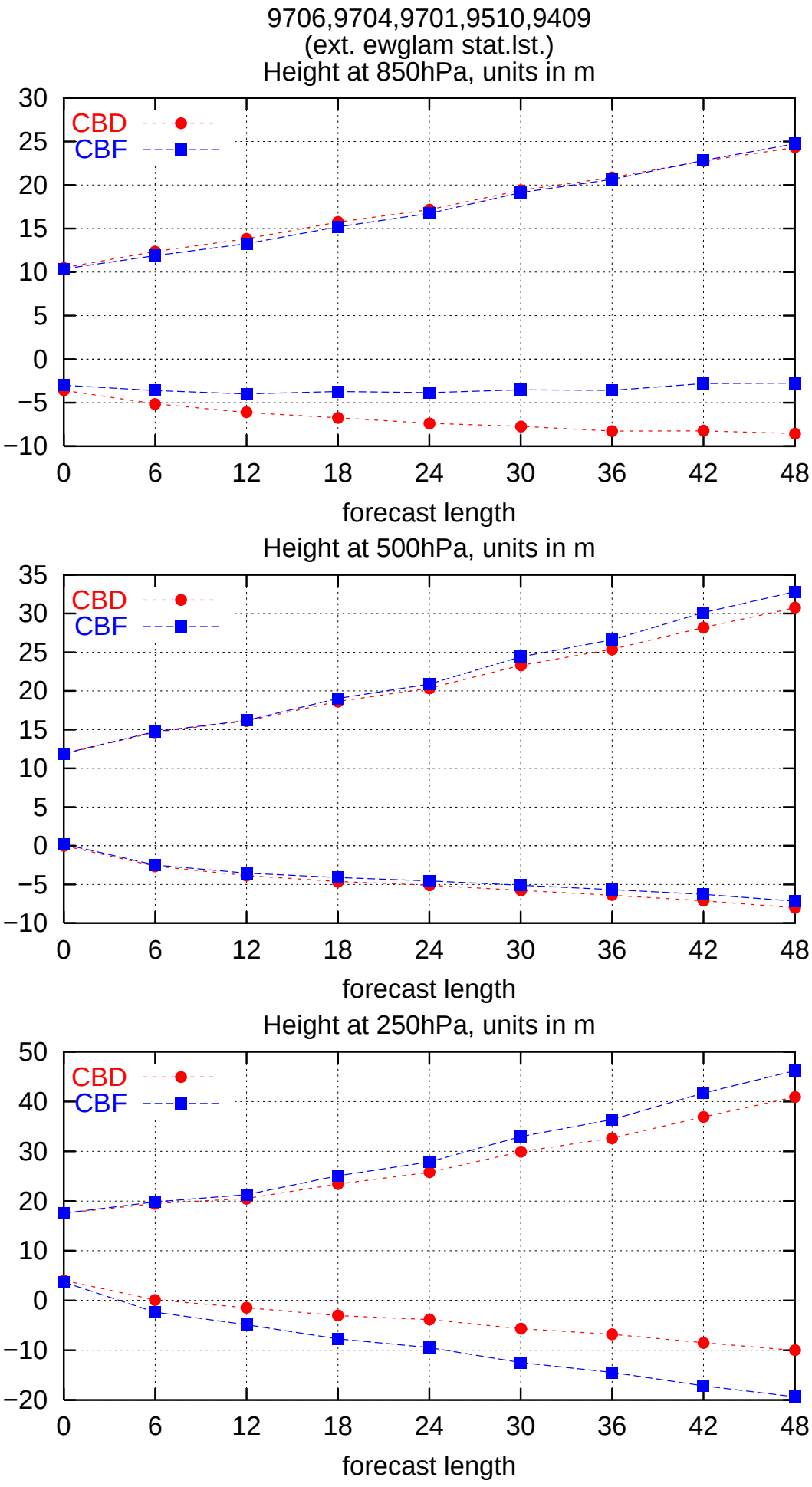

Figure 22: Obs verification of geopotential height at 850, 500 and 250 hPa level for Kuo/Cond Euler (CBD) versus Kuo/Cond semi-Lagrangian (CBF).

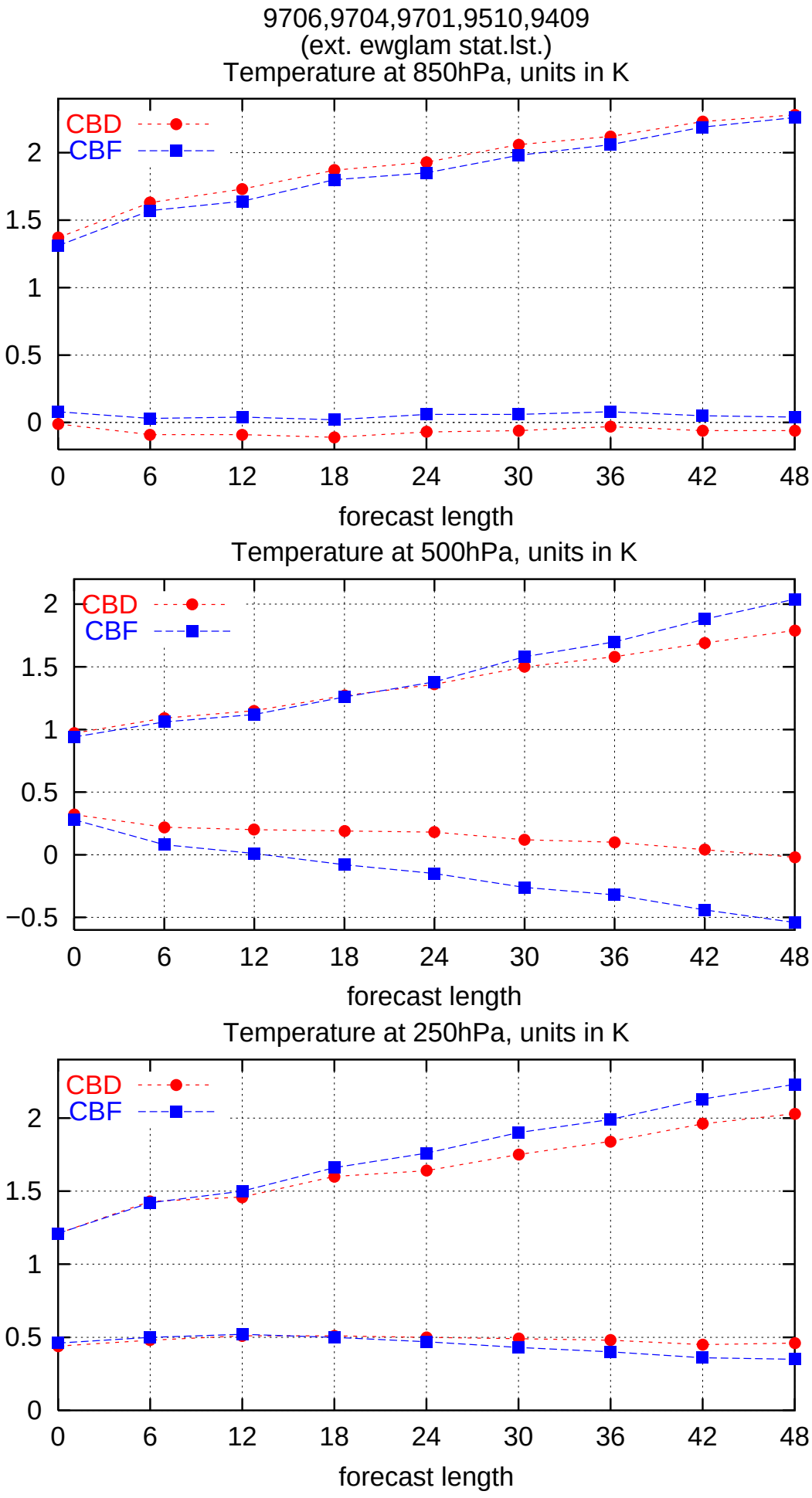

Figure 23: Obs verification of temperature at 850, 500 and 250 hPa level for Kuo/Cond Euler (CBD) versus Kuo/Cond semi-Lagrangian (CBF).

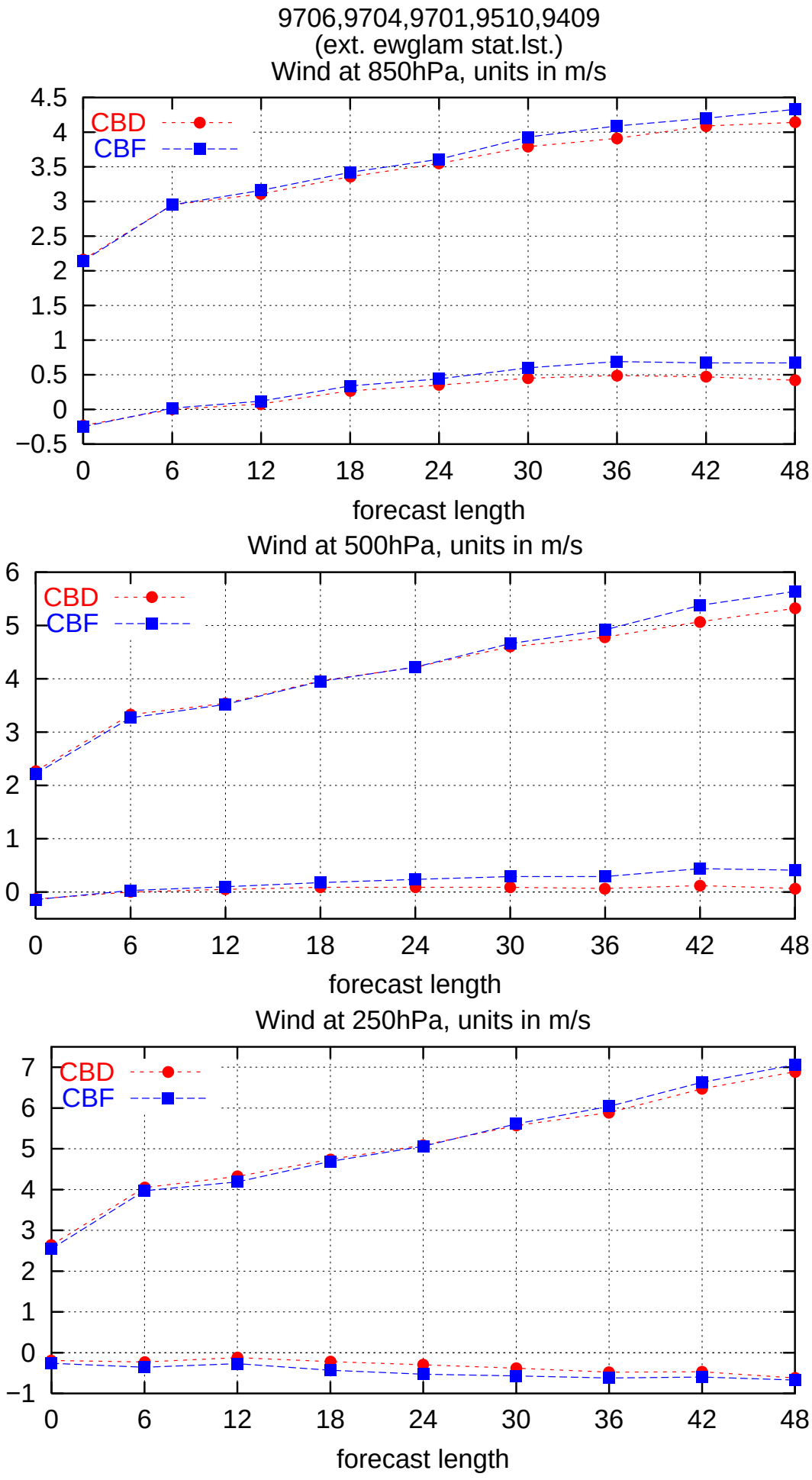

Figure 24: Obs verification of wind at 850, 500 and 250 hPa level for Kuo/Cond Euler (CBD) versus Kuo/Cond semi-Lagrangian (CBF).

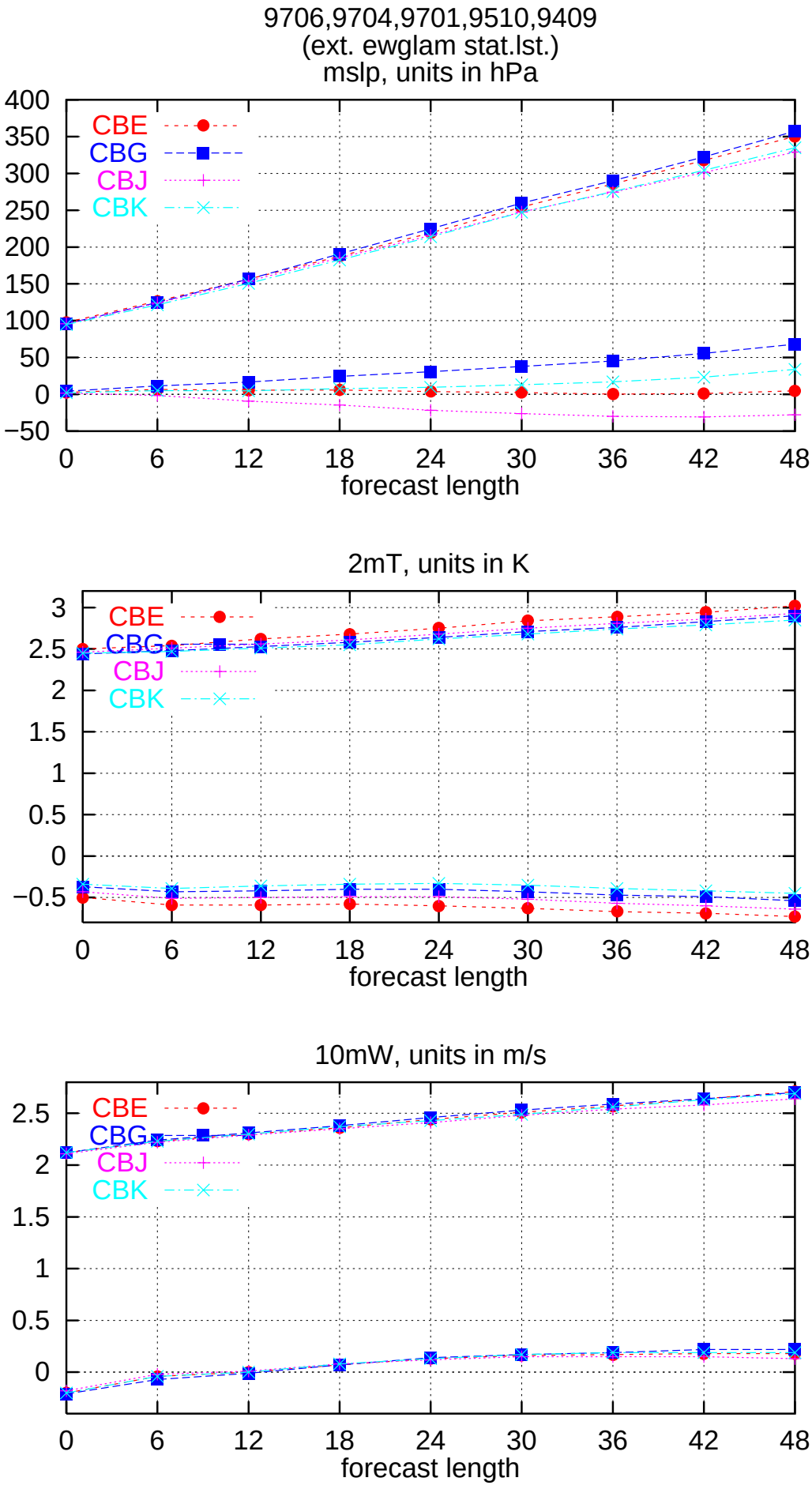

Figure 25: Obs verification of surface parameters for Sundqvist Euler (CBE), Sundqvist semi-Lagrangian (CBG), STRACO Euler (CBJ) and STRACO semi-Lagrangian (CBK).

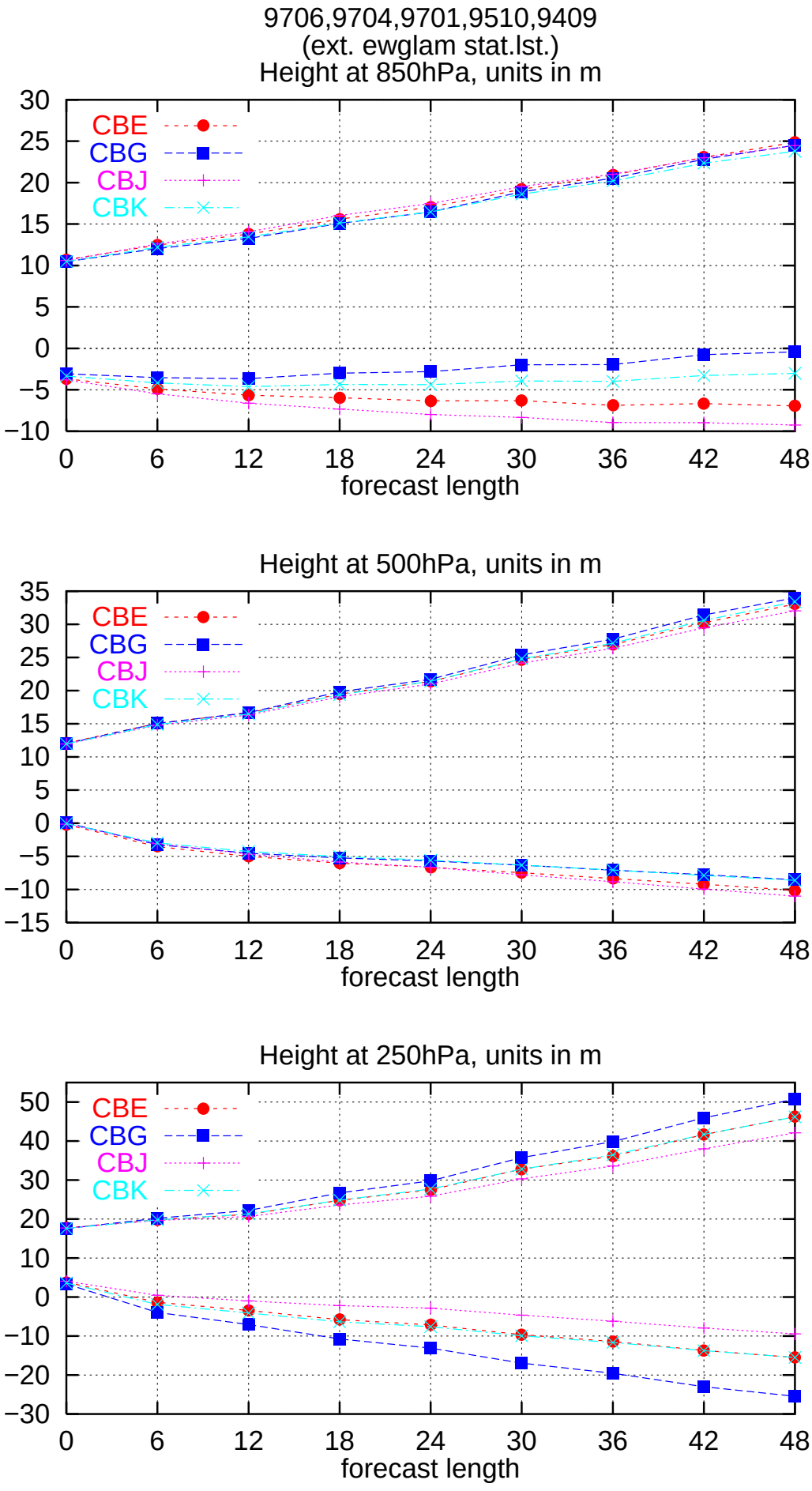

Figure 26: Obs verification of geopotential height at 850, 500 and 250 hPa level for Sundqvist Euler (CBE), Sundqvist semi-Lagrangian (CBG), STRACO Euler (CBJ) and STRACO semi-Lagrangian (CBK).

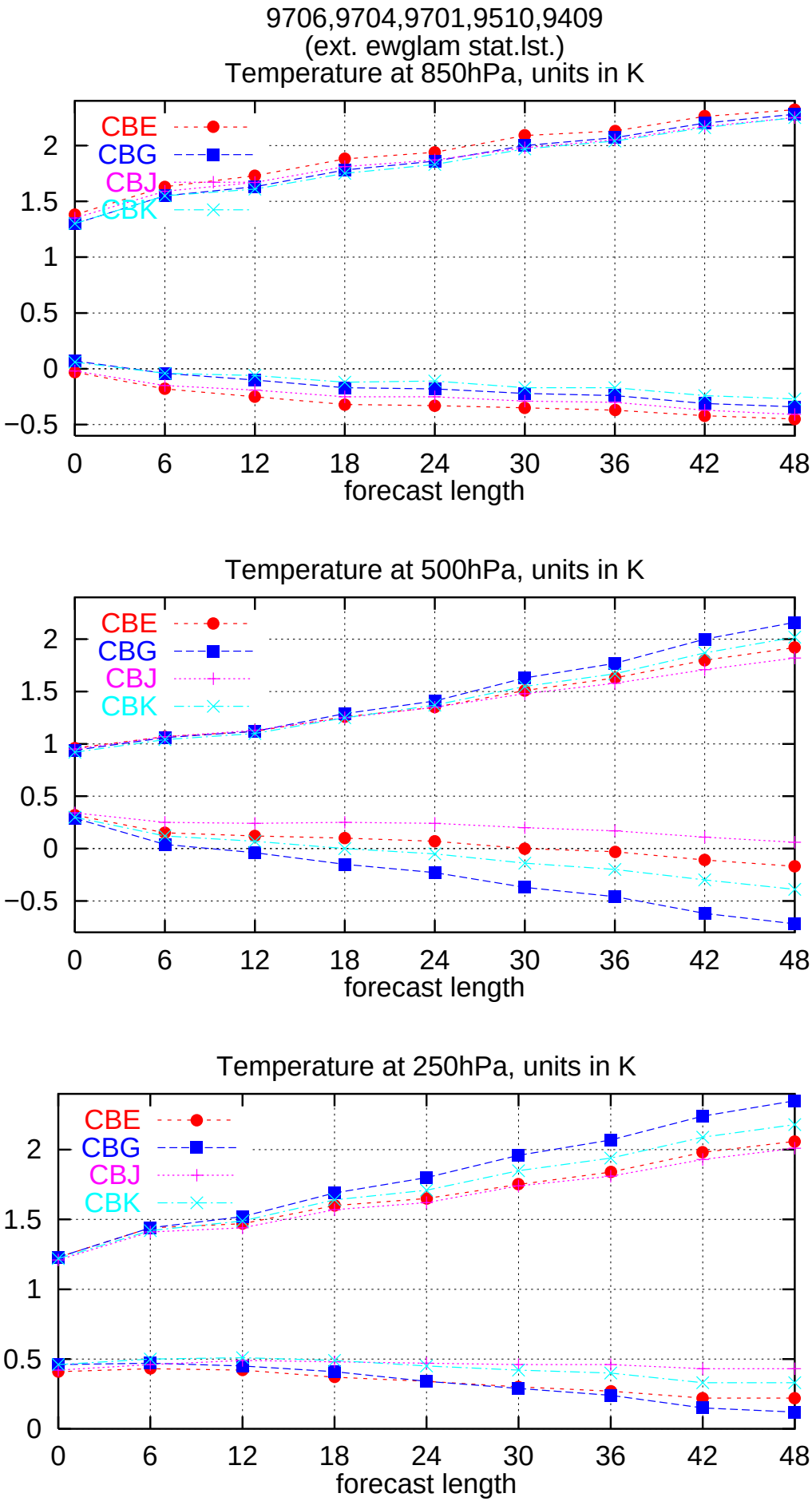

Figure 27: Obs verification of temperature at 850, 500 and 250 hPa level for Sundqvist Euler (CBE), Sundqvist semi-Lagrangian (CBG), STRACO Euler (CBJ) and STRACO semi-Lagrangian (CBK).

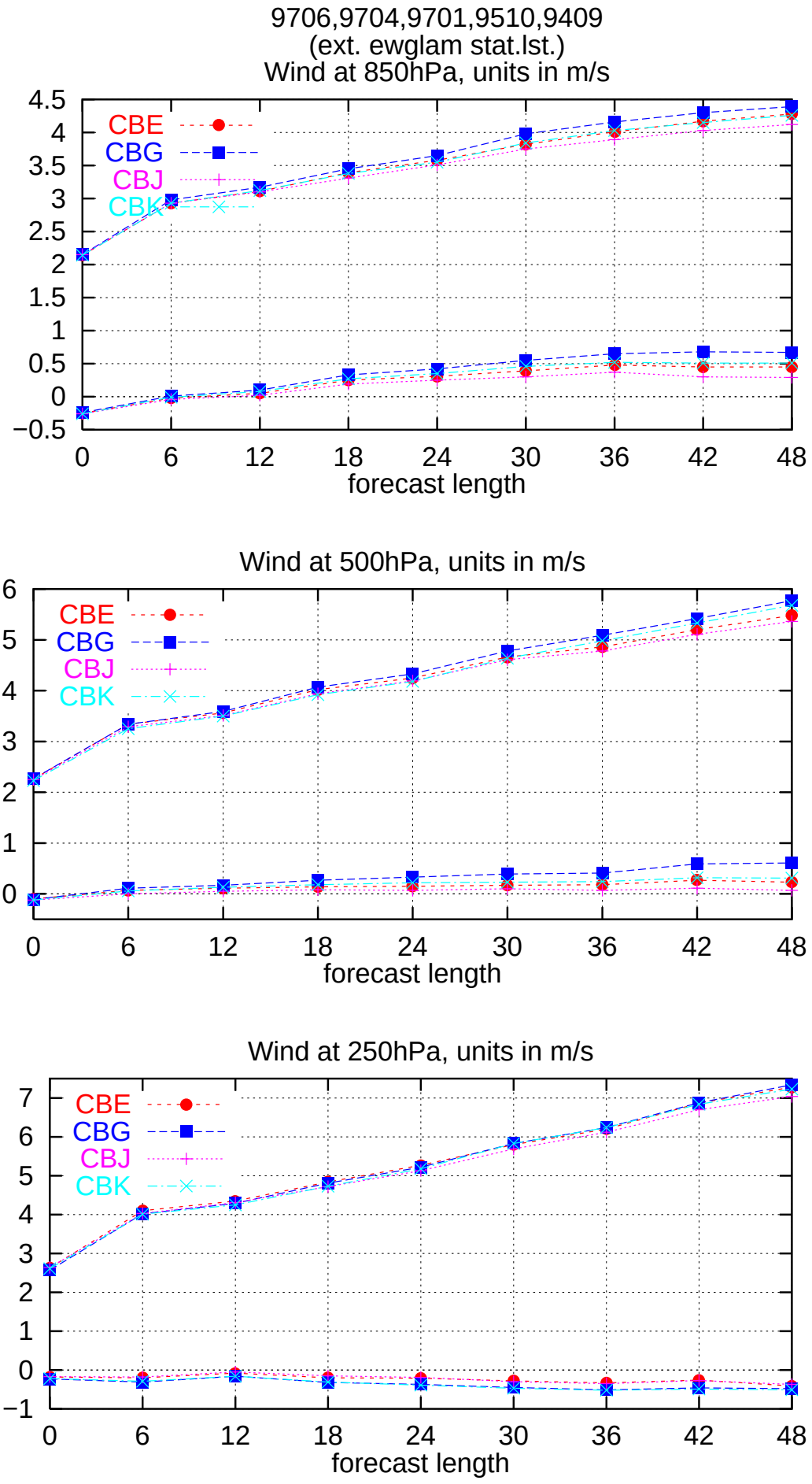

Figure 28: Obs verification of wind at 850, 500 and 250 hPa level for Sundqvist Euler (CBE), Sundqvist semi-Lagrangian (CBG), STRACO Euler (CBJ) and STRACO semi-Lagrangian (CBK).

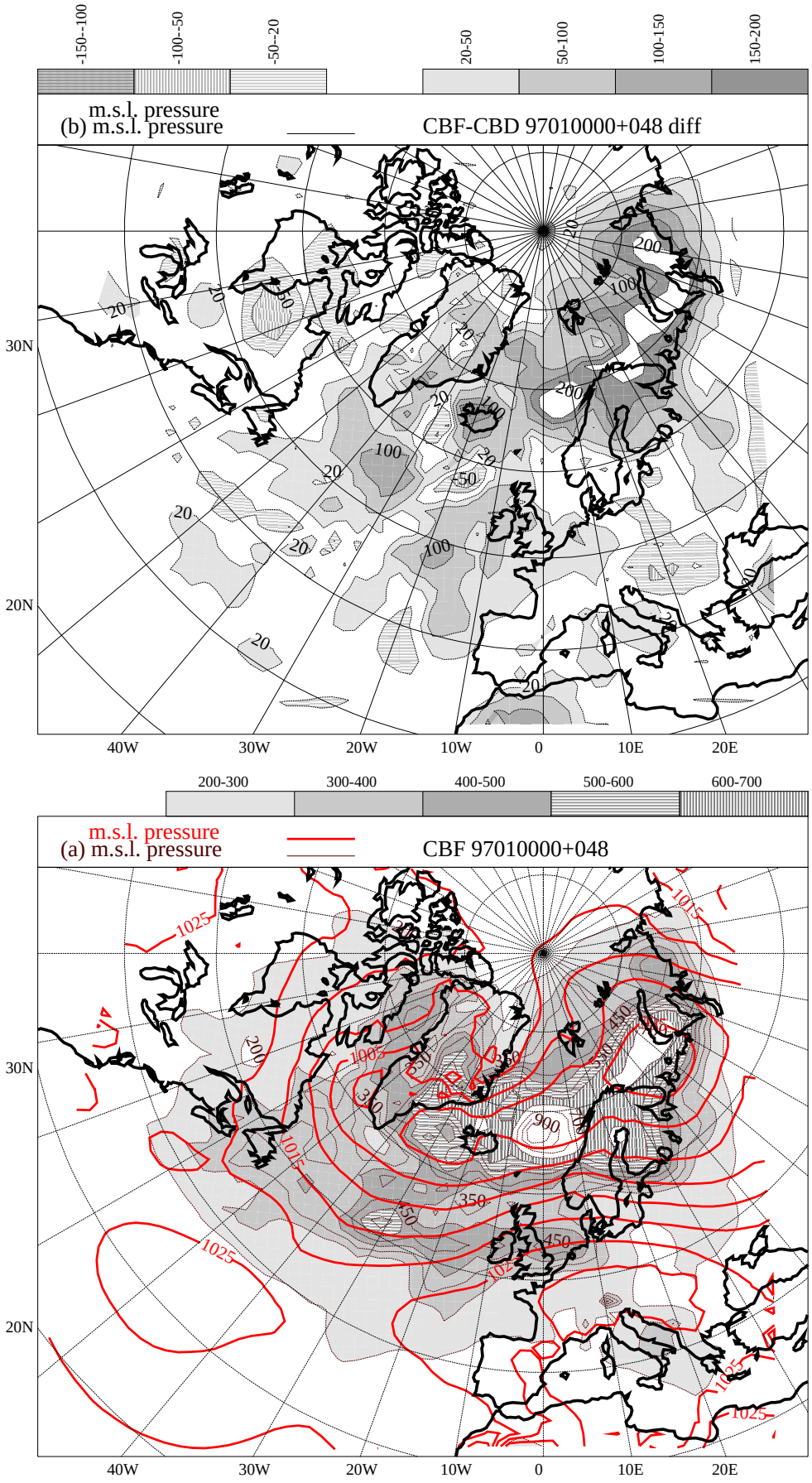

Figure 29: **(a)** Average mslp together with the std. dev. error of mslp for CBF in period P3. **(b)** For the same period the difference in std. dev. error of mslp between Kuo/Cond semi-Lagrangian (CBF) and Kuo/Cond Euler (CBD).

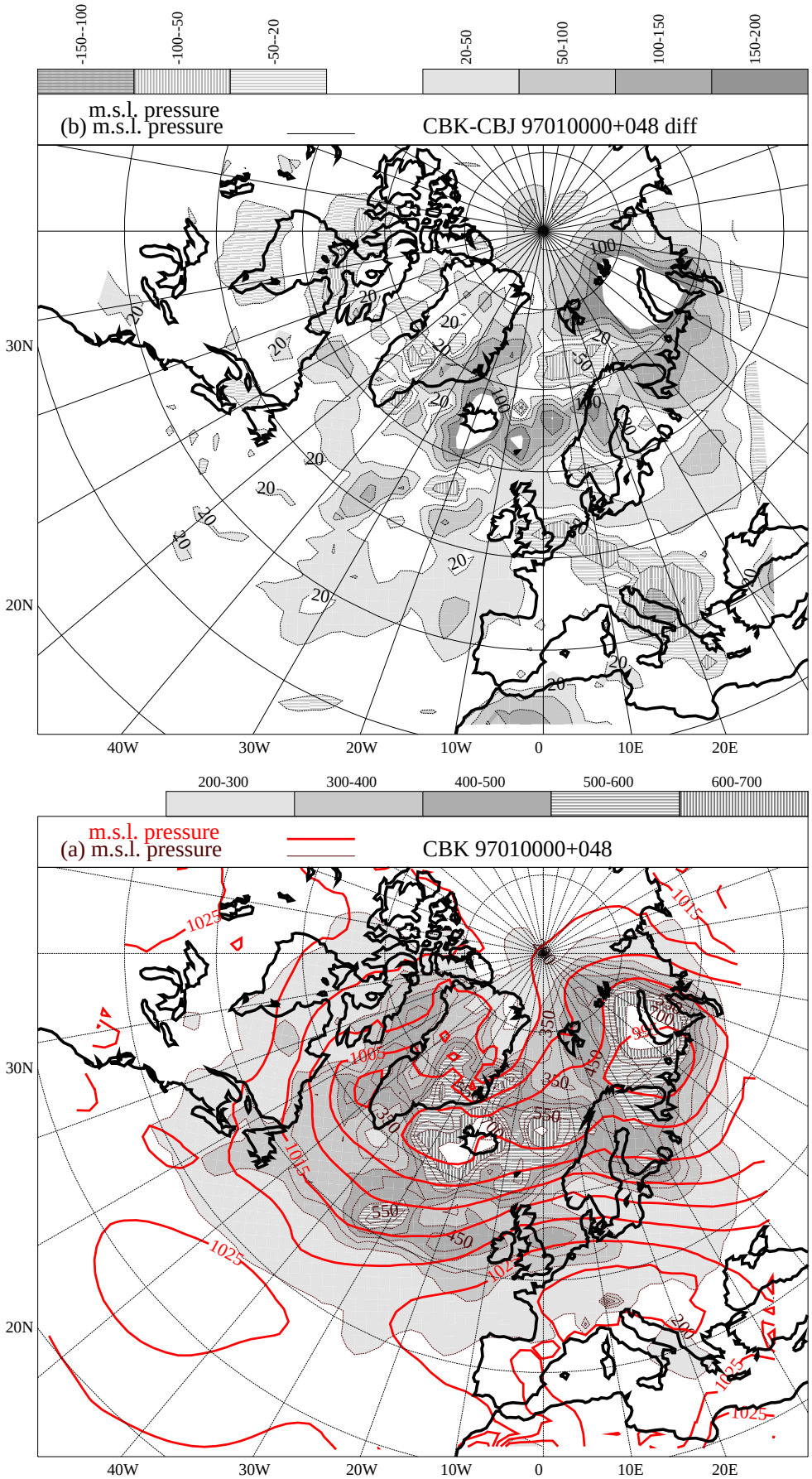

Figure 30: **(a)** Average mslp together with the std. dev. error of mslp for CBK in period P3. **(b)** For the same period the difference in std. dev. error of mslp between STRACO Euler (CBJ) and STRACO semi-Lagrangian (CBK).

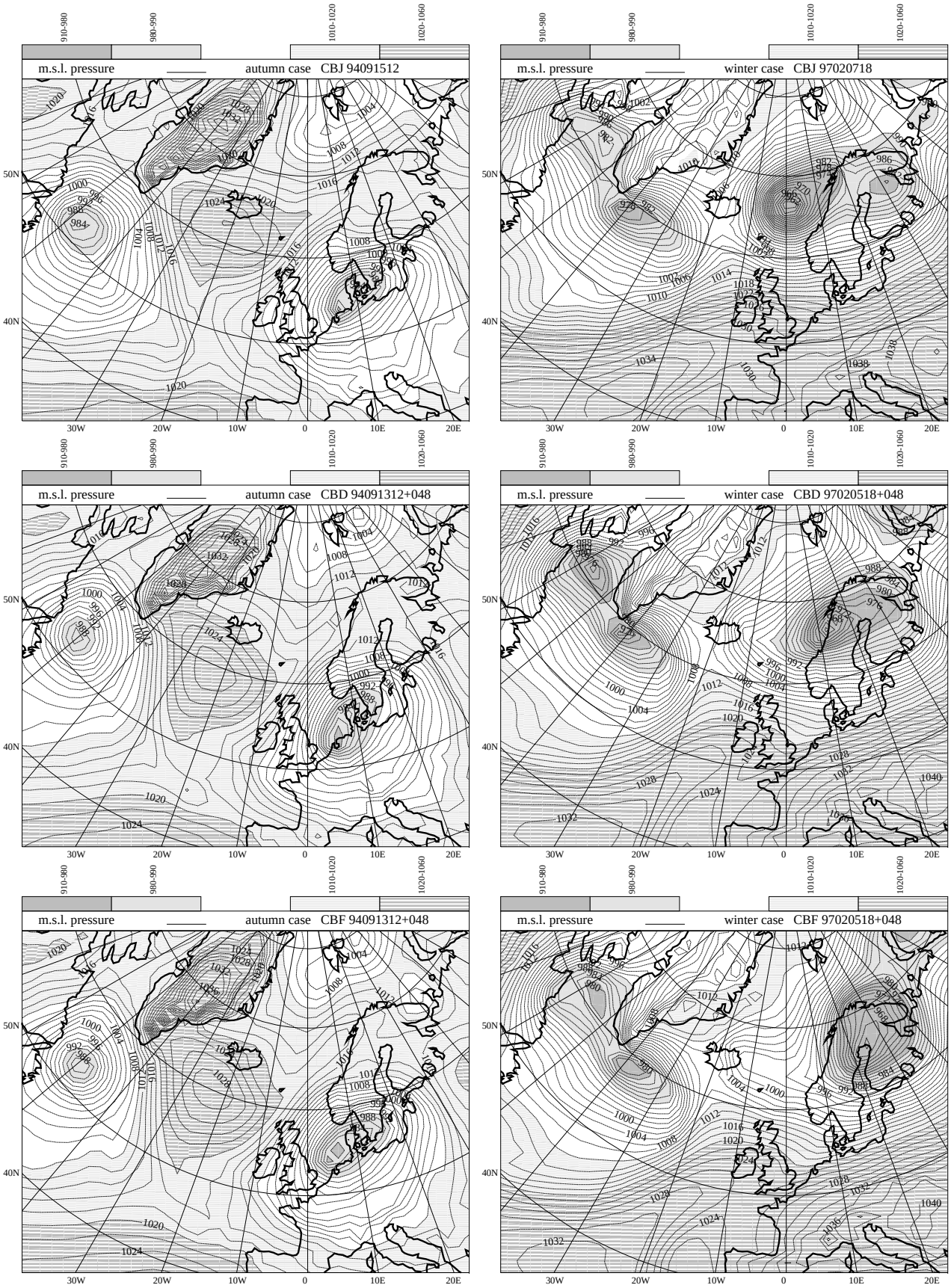

Figure 31: Autumn and winter case is for model versions with STRACO Euler (CBJ), Kuo/Cond Euler (CBD) and Kuo/Cond semi-Lagrangian. Shown are 48 hours forecasts forecasts together with the CBJ verifying analyses.

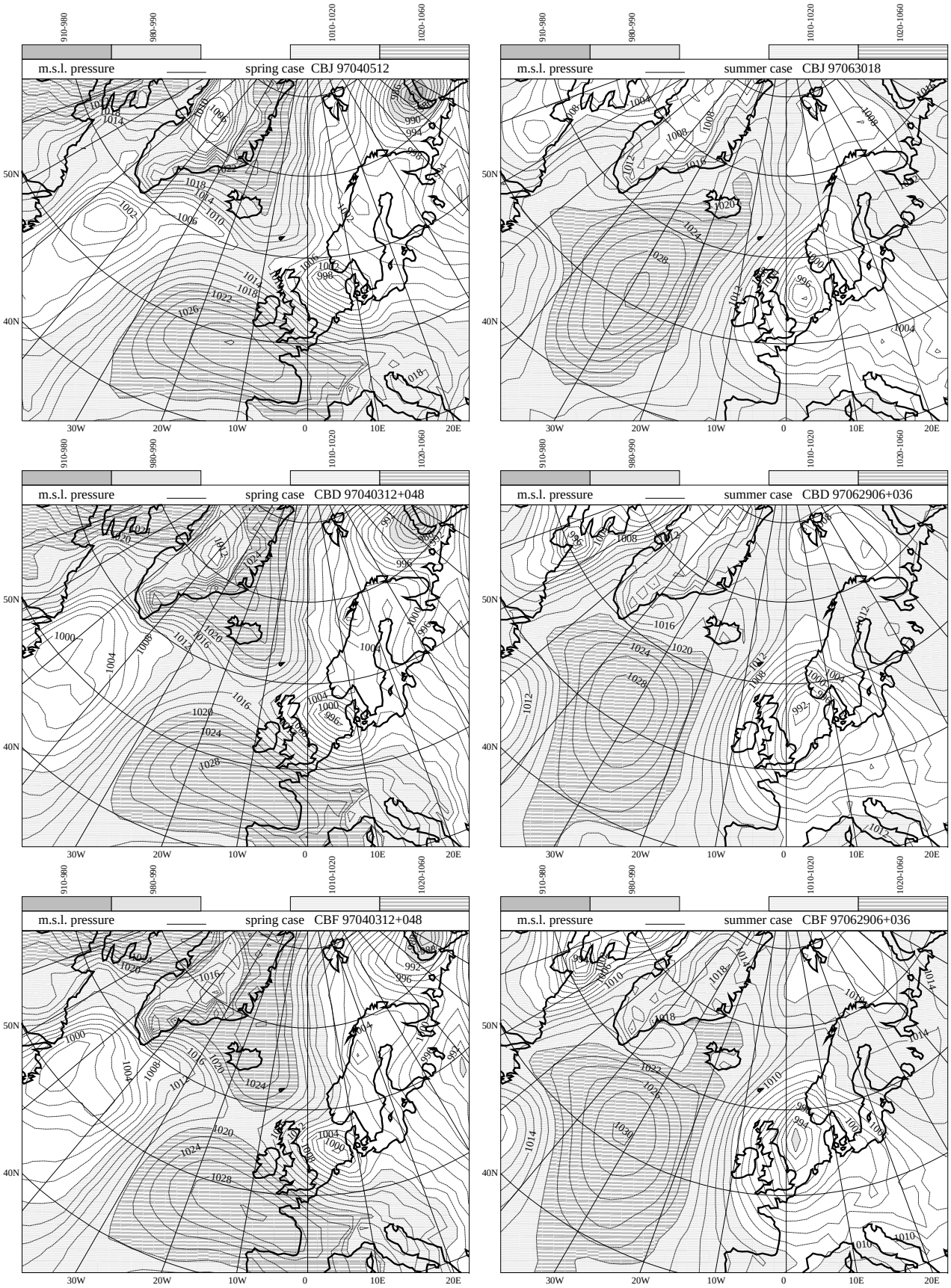

Figure 32: Spring and summer case is for model versions with STRACO Euler (CBJ), Kuo/Cond Euler (CBD) and Kuo/Cond semi-Lagrangian. Shown are 48 hours forecasts (spring case) and 36 hours forecasts (summer case) together with the CBJ verifying analyses.

DANISH METEOROLOGICAL INSTITUTE

Scientific Reports

Scientific reports from the Danish Meteorological Institute cover a variety of geophysical fields, i.e. meteorology (including climatology), oceanography, subjects on air and sea pollution, geomagnetism, solar-terrestrial physics, and physics of the middle and upper atmosphere.

Reports in the series within the last five years:

No. 94-1
Bjørn M. Knudsen: Dynamical processes in the ozone layer.

No. 94-2
J. K. Olesen and K. E. Jacobsen: On the atmospheric jet stream with clear air turbulences (CAT) and the possible relationship to other phenomena including HF radar echoes, electric fields and radio noise.

No. 94-3
Ole Bøssing Christensen and Bent Hansen Sass: A description of the DMI evaporation forecast project.

No. 94-4
I.S. Mikkelsen, B. Knudsen, E. Kyrö and M. Rummukainen: Tropospheric ozone over Finland and Greenland, 1988-94.

No. 94-5
Jens Hesselbjerg Christensen, Eigil Kaas, Leif Laursen: The contribution of the Danish Meteorological Institute (DMI) to the EPOCH project "The climate of the 21st century" No. EPOC-003-C (MB).

No. 95-1
Peter Stauning and T.J. Rosenberg: High-Latitude, Day-time Absorption Spike Events
1. Morphology and Occurrence Statistics.
Not Published.

No. 95-2
Niels Larsen: Modelling of changes in stratospheric ozone and other trace gases due to the emission changes : CEC Environment Program Contract No. EV5V-CT92-0079. Contribution to the final report.

No. 95-3
Niels Larsen, Bjørn Knudsen, Paul Eriksen, Ib Steen Mikkelsen, Signe Bech Andersen and Torben Stockflet Jørgensen: Investigations of ozone, aerosols, and clouds in the arctic stratosphere : CEC Environment Program Contract No. EV5V-CT92-0074. Contribution to the final report.

No. 95-4
Per Høeg and Stig Syndergaard: Study of the derivation of atmospheric properties using radio-occultation technique.

No. 95-5
Xiao-Ding Yu, **Xiang-Yu Huang** and **Leif Laursen** and Erik Rasmussen: Application of the HIRLAM system in China: Heavy rain forecast experiments in Yangtze River Region.

No. 95-6
Bent Hansen Sass: A numerical forecasting system for the prediction of slippery roads.

No. 95-7
Per Høeg: Proceeding of URSI International Conference, Working Group AFG1 Copenhagen, June 1995. Atmospheric Research and Applications Using Observations Based on the GPS/GLONASS System.

No. 95-8
Julie D. Pietrzak: A Comparison of Advection Schemes for Ocean Modelling.

No. 96-1
Poul Frich (co-ordinator), H. Alexandersson, J. Ashcroft, B. Dahlström, G.R. Demarée, A. Drebs, A.F.V. van Engelen, E.J. Førland, I. Hanssen-Bauer, R. Heino, T. Jónsson, K. Jonasson, L. Keegan, P.Ø. Nordli, **T. Schmith**, **P. Steffensen**, H. Tuomenvirta, O.E. Tveito: North Atlantic Climatological Dataset (NACD Version 1) - Final Report.

No. 96-2
Georg Kjærgaard Andreasen: Daily Response of High-latitude Current Systems to Solar Wind Variations: Application of Robust Multiple Regression. Methods on Godhavn magnetometer Data.

No. 96-3

Jacob Woge Nielsen, Karsten Bolding Kristensen, Lonny Hansen: Extreme sea level highs: A statistical tide gauge data study.

No. 96-4
Jens Hesselbjerg Christensen, Ole Bøssing Christensen, Philippe Lopez, Erik van Meijgaard, Michael Botzet: The HIRLAM4 Regional Atmospheric Climate Model.

No. 96-5
Xiang-Yu Huang: Horizontal Diffusion and Filtering in a Mesoscale Numerical Weather Prediction Model.

No. 96-6
Henrik Svensmark and Eigil Friis-Christensen:
Variation of Cosmic Ray Flux and Global Cloud Coverage - A Missing Link in Solar-Climate Relationships.

No. 96-7
Jens Havskov Sørensen and Christian Ødum Jensen: A Computer System for the Management of Epidemiological Data and Prediction of Risk and Economic Consequences During Outbreaks of Foot-and-Mouth Disease. CEC AIR Programme. Contract No. AIR3 - CT92-0652.

No. 96-8
Jens Havskov Sørensen: Quasi-Automatic of Input for LINCOM and RIMPUFF, and Output Conversion. CEC AIR Programme. Contract No. AIR3 - CT92-0652.

No. 96-9
Rashpal S. Gill and Hans H. Valeur:
Evaluation of the radarsat imagery for the operational mapping of sea ice around Greenland.

No. 96-10
Jens Hesselbjerg Christensen, Bennert Machenhauer, Richard G. Jones, Christoph Schär, Paolo Michele Ruti, Manuel Castro and Guido Visconti:
Validation of present-day regional climate simulations over Europe: LAM simulations with observed boundary conditions.

No. 96-11
Niels Larsen, Bjørn Knudsen, Paul Eriksen, Ib Steen Mikkelsen, Signe Bech Andersen and Torben Stockflet Jørgensen: European Stratospheric Monitoring Stations in the Artic: An European contribution to the Network for Detection of Stratospheric Change (NDSC): CEC Environment Programme Contract EV5V-CT93-0333: DMI contribution to the final report.

No. 96-12
Niels Larsen: Effects of heterogeneous chemistry on the composition of the stratosphere: CEC Environment Programme Contract EV5V-CT93-0349: DMI contribution to the final report.

No. 97-1
E. Friis Christensen og C. Skøtt: Contributions from the International Science Team. The Ørsted Mission - A Pre-Launch Compendium.

No. 97-2
Alix Rasmussen, Sissi Kiilsholm, Jens Havskov Sørensen, Ib Steen Mikkelsen: Analysis of Tropospheric Ozone Measurements in Greenland: Contract No. EV5V-CT93-0318 (DG 12 DTEE): DMI's contribution to CEC Final Report Arctic Trophospheric Ozone Chemistry ARCTOC.

No. 97-3
Peter Thejll: A Search for Effects of External Events on Terrestrial Atmospheric Pressure: Cosmic Rays

No. 97-4
Peter Thejll: A Search for Effects of External Events on Terrestrial Atmospheric Pressure: Sector Boundary Crossings

No. 97-5
Knud Lassen: Twentieth Century Retreat of Sea-Ice in the Greenland Sea

No. 98-1
Niels Woetman Nielsen, Bjarne Amstrup, Jess U. Jørgensen:
HIRLAM 2.5 parallel tests at DMI:
Sensitivity to type of schemes for turbulence, moist processes and advection

No. 98-2
Per Høeg, Georg Bergeton Larsen, Hans-Henrik Benzon, Stig Syndergaard, Mette Dahl Mortensen:
The GPSOS project
Algorithm Functional Design and Analysis of ionosphere, Stratosphere and Troposphere Observations

No. 98-3
Dahl Mortensen, Mette; Per Høeg:
Satellite Atmosphere Profiling Retrieval in a Nonlinear Troposphere
Previously entitled: Limitations Induced by Multipath

No. 98-4

Dahl Mortensen, Mette Per Høeg:
Resolution Properties in Atmospheric Profiling with GPS

No. 98-5
Gill, R. S. and M. K. Rosengren
Evaluation of the Radarsat Imagery for the Operational Mapping of Sea Ice around Greenland in 1997.

No. 98-6
Gill, R. S., Valeur, H. H., Nielsen, P. and Hansen, K. Q.: Using ERS SAR images in the operational mapping of sea ice in the Greenland waters: final report for ESA-ESRIN's: pilot projekt no. PP2.PP2.DK2 and 2nd Announcement of opportunity for the exploitation of ERS data projekt No. AO2..DK 102.

No. 98-7
Høeg, Per et al.: GPS Atmosphere Profiling Methods and Error Assessments.

No. 98-8
Svensmark, H., N. Woetmann Nielsen and A.M. Sempreviva: Large Scale Soft and Hard Turbulent States of the Atmosphere.

No. 98-9
Lopez, Philippe, Eigil Kaas and Annette Guldberg: The Full Particle-In-Cell advection scheme in spherical geometry**.**

No. 98-10
Svensmark, H.: Influence of Cosmic Rays on Earth's Climate.

No. 98-11
Thejll, Peter and Henrik Svensmark: Notes on the method of normalized multivariate regression.

No. 98-12
Lassen. K: Extent of sea ice in the Greenland Sea 1977-1997: an extension of DMI Scientific Report 97-5

No. 98-13
Larsen, Niels; Adriani, Alberto and Donfrancesco, Guido Di: Microphysical analysis oof plar stratospheric clouds observed by Lidar at McMurco, Antarctica

No.98-14
Dahl Mortensen, Mette: The Back-Propagation Method for Inversion of Radio Occultation Data.